

Effects of angular-momentum-changing electron collisions and radiative corrections on dielectronic satellite spectra

V. L. Jacobs

*E.O. Hulbert Center for Space Research (Code 4170), Naval Research Laboratory,
Washington, D.C. 20375*

J. E. Rogerson

Plasma Radiation Branch (Code 4720), Plasma Physics Division, Naval Research Laboratory, Washington, D.C. 20375

M. H. Chen

Lawrence Livermore National Laboratory, P.O. Box 808, Livermore, California 94550

R. D. Cowan

*Los Alamos National Laboratory (T-4), Mail Stop MS-B212, Los Alamos, New Mexico 87545
(Received 20 June 1985)*

The conventional low-density isolated-resonance theory for the intensities and widths of the $2l'2l'' \rightarrow 1s2l$ and the $1s2l'2l'' \rightarrow 1s^22l$ dielectronic satellite lines has been generalized to take into account angular-momentum-changing electron collisions and the interaction between the atomic system and the quantized radiation field. The electron collisional transitions alter the population densities of the autoionizing levels, while the atom-field interaction modifies the relative probabilities for autoionization and radiative decay. The modifications to the conventional low-density expression for the satellite-line intensities may be interpreted as interference between the resonant and nonresonant electron continua together with radiative corrections. These modifications have been expressed in terms of the unperturbed decay rates, the photoionization cross sections, and the Fano line-profile parameters. Using the transition probabilities obtained from two different relativistic atomic structure codes, the K-shell satellite-line intensities and widths have been calculated for argon as functions of temperature and density, taking into account both dielectronic recombination and inner-shell-electron collisional excitation. The combined effects of relativity, radiative corrections, and angular-momentum-changing electron collisions are predicted to be most significant for radiative transitions from the $2p^{2,3}P$ and $1s2p^{2,2}P$ metastable autoionizing states, which give rise to satellite lines that are relatively weak at low densities but are among the most prominent spectral features in high-density plasmas.

I. INTRODUCTION

It was first established by Burgess¹ that dielectronic recombination is the dominant recombination mechanism for multiply charged atomic ions in low-density high-temperature laboratory and astrophysical plasmas. The dielectronic recombination process often gives rise to prominent satellite lines in the far-ultraviolet and x-ray emission spectra of both low-density^{2,3} and high-density^{4,5} plasmas. When these satellite lines are spectroscopically resolvable from the associated resonance line of the recombining ion, they can be utilized for the determination of the temperature, density, and state of ionization. While simplified calculations⁶ are expected to be adequate for the evaluation of the total recombination rate resulting from the multitude of satellite transitions, a detailed treatment, which is based on a rigorous quantum-mechanical theory, is obviously required for the accurate interpretation of the resolvable dielectronic satellite spectra. The present investigation has been devoted to the evaluation of improved quantum-mechanical expressions⁷ for the satellite-line intensities and widths.

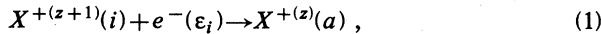
In order to develop a rigorous quantum-mechanical theory of dielectronic recombination, it is necessary to treat in a unified manner both the interaction between

electrons and the interaction between the atomic system and the quantized radiation field. This unified treatment can be accomplished by utilizing the methods of multichannel collision theory and quantum electrodynamics. Unified quantum-mechanical treatments of electron-ion recombination accompanied by photon emission, which describe both the resonant and nonresonant recombination processes together with their interference, have been presented by Davies and Seaton,⁸ by Bell and Seaton,⁹ and by Shore.¹⁰ However, approximations to the scattering matrix have been used in these investigations, leading to expressions in which the autoionization and radiative decay rates are additive.

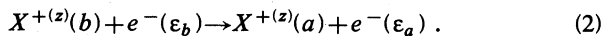
Armstrong, Theodosiou, and Wall¹¹ were the first to investigate the effects of the electromagnetic interaction between the final continuum states which result from the autoionization and radiative decay modes. They demonstrated that the final-state interaction can alter the Auger and fluorescence probabilities. They were able to recast the expressions for the perturbed decay probabilities into the familiar branching-ratio forms by introducing effective decay rates, which can be expressed in terms of the unperturbed decay rates and the matrix elements that describe the nonresonant photoionization and radiative recombination processes. The results obtained by

Armstrong, Theodosiou, and Wall¹¹ were subsequently rederived by Haan and Cooper,¹² using elegant Møller scattering-operator techniques, and shown to have a wider region of validity than originally recognized. The theory of this final-state interaction has recently been extended⁷ to take into account the angular-momentum degeneracy of the atomic levels and the multiplicity of angular-momentum components in the partial-wave expansion for the electron-continuum state. The isolated-resonance approximation was then employed to obtain modified expressions for the intensities of the satellite lines which are produced by the radiative decay of autoionizing states of multiply charged ions in low-density plasmas.

In the conventional corona-model theory of dielectronic satellite-line intensities,^{13,14} which is valid for sufficiently low plasma densities, it is assumed that all excited states of the atomic system are depopulated only by autoionization or spontaneous radiative decay processes. The autoionizing state $|a\rangle$ of the ion $X^{+(z)}$ with residual charge z can be populated either by the radiationless electron-capture process,



or, alternatively, as a result of the inner-shell-electron collisional excitation process,



If the decay rate for the spontaneous radiatively stabilizing transition

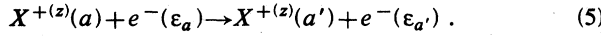


is denoted by $A_r(a \rightarrow f)$, the rate per unit volume of photon emission in the satellite transition $|a\rangle \rightarrow |f\rangle$ is given by

$$I(a \rightarrow f) = A_r(a \rightarrow f) \left[\sum_i \frac{C_{\text{cap}}(i \varepsilon_i \rightarrow a) N(i) N_e}{A_a(a) + A_r(a)} + \sum_b \frac{C_e(b \rightarrow a) N(b) N_e}{A_a(a) + A_r(a)} \right], \quad (4)$$

where the electron-temperature-dependent capture and inner-shell-electron collisional excitation-rate coefficients are denoted by $C_{\text{cap}}(i \varepsilon_i \rightarrow a)$ and $C_e(b \rightarrow a)$, respectively, and the decay rates resulting from all permissible autoionization and spontaneous radiative emission processes are denoted by $A_a(a)$ and $A_r(a)$, respectively. The number densities of ions in the states $|i\rangle$ and $|b\rangle$ are denoted by $N(i)$ and $N(b)$, respectively, and N_e is the electron density.

The conventional corona-model theory of dielectronic satellite-line intensities has been generalized¹⁵ to take into account the electron collisional transitions



Burgess and Summers¹⁶ first suggested that the intensity of the unresolvable dielectronic recombination satellite lines could be enhanced by angular-momentum-changing collisions involving the Rydberg autoionizing states. A significant amplification in the unresolvable dielectronic recombination satellite intensity has now been predicted

by two independent calculations,^{17,18} in which account was taken of the collision processes induced by plasma ions, and also by an alternative treatment¹⁹ of plasma-density effects, in which the quasistatic action of the plasma ions was described by a uniform static electric field distribution. The generalized theory of dielectronic satellite intensities has predicted¹⁵ that the plasma electrons are capable of amplifying the intensities of the resolvable satellite lines, which are produced by radiative transitions from the low-lying autoionizing levels. We now present a unified treatment of angular-momentum-changing electron collisions and radiative corrections for resolvable satellite spectra.

The remainder of this paper is organized in the following manner. In Sec. II, the theory of the final-state interaction is reviewed and expressions for the altered autoionization and radiative decay probabilities are presented. The isolated-resonance approximation is then employed to obtain the modified expressions for the satellite-line intensities produced by dielectronic recombination and inner-shell-electron collisional excitation in low-density plasmas. The theory of electron collisional transitions is discussed in Sec. III, where generalized expressions are obtained for the satellite-line intensities resulting from radiationless electron capture and collisional excitation of an inner-shell electron. The theory of the satellite-line shapes is then developed in the isolated-line approximation, taking into account the same autoionization, radiative decay, and electron collisional processes which are included in the determination of the population densities of the autoionization levels. The description and results of our calculations are presented in Sec. IV, where the importance of radiative corrections is discussed for satellite-line intensities in both low- and high-density plasmas. Finally, our conclusions are presented in Sec. V.

II. THEORY OF RADIATIVE CORRECTIONS

We consider an excited state $|a\rangle$ of an atomic system which can decay either by an autoionization process to a state $|i\rangle$ of the residual ion, emitting an electron with momentum \mathbf{p} , or by a spontaneous radiative transition to a state $|f\rangle$, emitting a photon with momentum \mathbf{k} . The direct-product states denoted by $|a,0\rangle$, $|i,0\rangle$, and $|f,\mathbf{k}\rangle$ are eigenstates of the unperturbed Hamiltonian H^0 , which is the sum of the unperturbed atomic Hamiltonian H_A and the Hamiltonian H_F for the free-radiation field. Within the restricted subspace of this one-discrete-level two-continua basis, an exact closed-form solution can be obtained^{7,12} for the eigenstates of the complete Hamiltonian consisting of the combined atomic and quantized-radiation-field Hamiltonians plus the atom-field interaction H_{AF} . This electromagnetic interaction couples the final-state continuum channels corresponding to the unperturbed autoionization and radiative decay modes. Armstrong, Theodosiou, and Wall¹¹ first derived the modifications to the Auger and fluorescence branching ratios which result from this final-state interaction. An essential new feature of their approach is the unified treatment of the interactions responsible for autoionization and for radiative decay.

A. Autoionization and radiative decay probabilities

The spectral amplitudes describing the autoionization and radiative decay processes are given by the projections of the unperturbed initial autoionizing state onto the exact continuum eigenstates of the complete Hamiltonian which satisfy the required incoming spherical wave boundary conditions. If the electron-spin projection and photon-polarization quantum numbers are denoted by m_s and λ , respectively, the exact autoionization and radiative decay probabilities may be defined by

$$P_a(a \rightarrow i\epsilon_i) = \sum_{M_a} \sum_{M_i} \sum_{m_s} \int d^3 p \frac{|\langle i\mathbf{p} m_s, 0^- | a, 0 \rangle|^2}{2J_a + 1} \quad (6)$$

and

$$P_r(a \rightarrow f) = \sum_{M_a} \sum_{M_f} \sum_{\lambda} \int d^3 k \frac{|\langle f, \mathbf{k} \lambda^- | a, 0 \rangle|^2}{2J_a + 1}, \quad (7)$$

which are averaged over the initial magnetic substates specified by M_a , summed over the final polarizations, and integrated over the final momenta.

The conventional expressions for the Auger and fluorescence branching ratios are simply given by^{13,14}

$$P_a(a \rightarrow i\epsilon_i) = \frac{A_a(a \rightarrow i\epsilon_i)}{A_a(a \rightarrow i\epsilon_i) + A_r(a \rightarrow f)} \quad (8)$$

and

$$P_r(a \rightarrow f) = \frac{A_r(a \rightarrow f)}{A_a(a \rightarrow i\epsilon_i) + A_r(a \rightarrow f)}, \quad (9)$$

where $A_a(a \rightarrow i\epsilon_i)$ and $A_r(a \rightarrow f)$ are the autoionization and radiative decay rates in the absence of the final-state continuum-continuum interaction. If we now denote the exact branching ratios and the effective decay rates in the presence of the final-state interaction by using the tilde, the exact branching ratios may be expressed in the same familiar forms

$$\tilde{P}_a(a \rightarrow i\epsilon_i) = \frac{\tilde{A}_a(a \rightarrow i\epsilon_i)}{\tilde{A}_a(a \rightarrow i\epsilon_i) + \tilde{A}_r(a \rightarrow f)} \quad (10)$$

and

$$\tilde{P}_r(a \rightarrow f) = \frac{\tilde{A}_r(a \rightarrow f)}{\tilde{A}_a(a \rightarrow i\epsilon_i) + \tilde{A}_r(a \rightarrow f)}. \quad (11)$$

For the problem with one discrete level and two continuum channels, the effective decay rates which are obtained in the pole approximation¹² can be expressed in the forms⁷

$$\begin{aligned} \tilde{A}_a(a \rightarrow i\epsilon_i) = & \frac{A_a(a \rightarrow i\epsilon_i)}{\Psi^2} \left[\Psi^2 - \frac{2\Psi A_r(a \rightarrow f)}{Q_f^2 A_a(a \rightarrow i\epsilon_i)} \right. \\ & + (\Psi - 1) \left[1 + \frac{1}{Q_f^2} \right] \\ & \times \left. \frac{A_r(a \rightarrow f)}{A_a(a \rightarrow i\epsilon_i)} \right] \end{aligned} \quad (12)$$

and

$$\tilde{A}_r(a \rightarrow f) = \frac{A_r(a \rightarrow f)}{\Psi^2} \left[1 + \frac{1}{Q_f^2} \right]. \quad (13)$$

The continuum-continuum coupling parameter Ψ may be related to the cross section for photoionization from the state $|f\rangle$ or, alternatively, to the cross section for the inverse radiative recombination process $|ip, 0\rangle \rightarrow |f, \mathbf{k}\rangle$. The multichannel Fano line-profile parameter²⁰ is denoted by Q_f . In Sec. IV, the parameters Ψ and Q_f will be defined in terms of the various transition matrix elements. When the final-state interaction involves only a single term in the partial-wave expansion for the electron-continuum state, the expressions obtained for the effective decay rates can be reduced to the results derived previously.^{11,12} In general, the expressions (12) and (13) contain terms corresponding to the interference between different partial-wave components of the electron-continuum state.

In order to treat the most complex dielectronic recombination process which can occur in a plasma, the theory of the Auger and fluorescence probabilities must be further extended to allow for autoionization into a set of states $|i\rangle$ of the residual ion and also for spontaneous radiative transitions into a set of final atomic states $|f\rangle$. These generalizations have been previously reported,^{7,11} and we will require in the present investigation only the extension of the theory for several photon-continuum states $|f, \mathbf{k}_f \lambda_f\rangle$. The Auger and fluorescence branching ratios in the presence of the final-state interactions are now expressible in the forms

$$\tilde{P}_a(a \rightarrow i\epsilon_i) = \frac{\tilde{A}_a(a \rightarrow i\epsilon_i)}{\tilde{A}_a(a \rightarrow i\epsilon_i) + \sum_f \tilde{A}_r(a \rightarrow f)} \quad (14)$$

and

$$\tilde{P}_r(a \rightarrow f) = \frac{\tilde{A}_r(a \rightarrow f)}{\tilde{A}_a(a \rightarrow i\epsilon_i) + \sum_f \tilde{A}_r(a \rightarrow f)}. \quad (15)$$

When the continuum-continuum couplings involve only a single term in the partial-wave expansion for the electron-continuum state, the effective decay rates are given by^{7,11}

$$\begin{aligned} \tilde{A}_a(a \rightarrow i\epsilon_i) = & \frac{A_a(a \rightarrow i\epsilon_i)}{\Psi^2} \\ & \times \left[1 + \left(\frac{1}{A_a(a \rightarrow i\epsilon_i)} \sum_f \frac{A_r(a \rightarrow f)}{Q_f} \right)^2 \right] \end{aligned} \quad (16)$$

and

$$\tilde{A}_r(a \rightarrow f) = \frac{A_r(a \rightarrow f)}{\Psi^2} \left\{ \frac{1}{Q_f^2} + \left[1 + \frac{1}{A_a(a \rightarrow i\varepsilon_i)} \sum_{f'} \frac{A_r(a \rightarrow f')}{Q_{f'}} \left(\frac{Q_f - Q_{f'}}{Q_{f'}} \right)^2 \right] \right\}. \quad (17)$$

B. Dielectronic satellite-line intensities for low-density plasmas

In order to determine the spectral-line intensities associated with the radiative decay of autoionizing states of atomic ions in plasmas, it is necessary to take into account the collision processes by means of which these states can be excited. Although photoexcitation processes are expected to be important in the presence of intense radiation fields, autoionizing states in most laboratory and astrophysical plasmas are produced predominantly by electron-ion collisions. The evaluation of the scattering matrix for the resonant electron-ion collision process is most easily carried out in the Breit-Wigner isolated-resonance approximation, in which the linewidth is assumed to be small in comparison with the energy separation between adjacent levels. In the isolated-resonance approximation, the resonant cross section for recombination accompanied by radiative emission can be expressed as the product of the radiationless electron-capture cross section and the probability of decay into the photon-continuum channel.

In the dielectronic recombination process, the autoionizing state $|a\rangle$ is excited by the radiationless electron-capture process represented by Eq. (1), which corresponds to the inverse of autoionization. If the rate coefficient describing the radiationless electron-capture process in the presence of the final-state interaction is denoted by $\tilde{C}_{cap}(i\varepsilon_i \rightarrow a)$, the rate of radiative emission per unit electron density is given by the dielectronic recombination radiation rate coefficient

$$\tilde{C}_r(b \rightarrow a) = \frac{32}{\sqrt{3}} \pi^{3/2} \frac{(2J_a+1)}{(2J_b+1)} \left[\frac{a_0}{\alpha} \right]^{3/2} \left[\frac{E_H}{\Delta E(a \rightarrow b)} \right]^{-2} \times \left[\frac{\sqrt{3}}{2\pi} \right] \left[(1n4) \exp \left[-\frac{\Delta E(a \rightarrow b)}{k_B T_e} \right] + E_1 \left[\frac{\Delta E(a \rightarrow b)}{k_B T_e} \right] \right], \quad (21)$$

which involves the perturbed spontaneous emission rates $\tilde{A}_r(a \rightarrow b)$ for the electric dipole transitions $|a\rangle \rightarrow |b\rangle$.

The total low-density dielectronic satellite-line intensity $\tilde{I}(a \rightarrow f)$ produced by both radiationless electron captures and inner-shell-electron collisional excitations is therefore determined by evaluating the expression obtained from Eq. (4) after all spontaneous decay rates and collisional excitation rate coefficients have been replaced by their values in the presence of the final-state interaction.

III. THEORY OF ELECTRON COLLISIONAL TRANSITIONS

The effects of electron-induced collisional transitions between the autoionizing levels have been investigated for heliumlike satellite lines by Vinogradov, Skobelev, and Yukov²² and by Seely.²³ The analogous collisional pro-

$$\tilde{\alpha}_{DR}(i\varepsilon_i \rightarrow a \rightarrow f) = \tilde{C}_{cap}(i\varepsilon_i \rightarrow a) \tilde{P}_r(a \rightarrow f), \quad (18)$$

where $\tilde{P}_r(a \rightarrow f)$ denotes the probability for radiative emission during the satellite transition $a \rightarrow f$ in the presence of the final-state interaction. For a Maxwellian distribution of incident electron velocities, the radiationless capture rate coefficient can be expressed in terms of the autoionization rate $\tilde{A}_a(a \rightarrow i\varepsilon_i)$ by means of the detailed balance relationship¹³

$$\begin{aligned} \tilde{C}_{cap}(i\varepsilon_i \rightarrow a) &= 2^3 a_0^3 \pi^{3/2} \frac{2J_a+1}{2(2J_i+1)} \left[\frac{E_H}{k_B T_e} \right]^{3/2} \\ &\times \exp \left[-\frac{E(a) - E(i)}{k_B T_e} \right] \tilde{A}_a(a \rightarrow i\varepsilon_i). \end{aligned} \quad (19)$$

An additional mechanism for populating the autoionizing state $|a\rangle$ is the electron-impact excitation from the bound state $|b\rangle$ of the atomic system. The transition $|b\rangle \rightarrow |a\rangle$ corresponds to the excitation of an inner-shell electron. If the electron-impact excitation rate coefficient is denoted by $\tilde{C}_e(b \rightarrow a)$, the radiative emission rate per unit electron density is given by the inner-shell-electron excitation radiation rate coefficient

$$\tilde{C}_r(b \rightarrow a \rightarrow f) = \tilde{C}_e(b \rightarrow a) \tilde{P}_r(a \rightarrow f). \quad (20)$$

In the calculations reported in our investigation, the collisional excitation rate coefficients $\tilde{C}_e(b \rightarrow a)$ in the presence of the final-state interaction have been evaluated in the Bethe approximation²¹

$$\begin{aligned} \tilde{A}_r(a \rightarrow b) &= \left(\frac{E_H}{k_B T_b} \right)^{3/2} \left(\frac{k_B T_e}{\Delta E(a \rightarrow b)} \right) \\ &\times \left[\frac{\sqrt{3}}{2\pi} \right] \left[(1n4) \exp \left[-\frac{\Delta E(a \rightarrow b)}{k_B T_e} \right] + E_1 \left[\frac{\Delta E(a \rightarrow b)}{k_B T_e} \right] \right], \end{aligned} \quad (21)$$

cesses in lithiumlike ions have been taken into account by Jacobs and Blaha.¹⁵ Duston *et al.*²⁴ have recently calculated the intensities of both the heliumlike and the lithiumlike satellite lines, taking into account these electron collisional transitions as well as electron collisional ionization and recombination processes involving the autoionizing levels, which can appreciably alter their populations only at very high densities. In this section, we present an extension of the approach described by Jacobs and Blaha¹⁵ in which we treat the combined effects of electron collisional transitions and radiative corrections for both heliumlike and lithiumlike satellite lines.

A. Dielectronic satellite-line intensities

The total rate $W(a \rightarrow a')$ describing transitions between the autoionizing levels resulting from collisional and

spontaneous radiative processes is given by

$$W(a \rightarrow a') = N_e C_e(a \rightarrow a') + \sum_h N_h C_h(a \rightarrow a') + A_r(a \rightarrow a') \Theta(E_a - E'_a), \quad (22)$$

where $C_e(a \rightarrow a')$ is the electron collisional rate coefficient and $C_h(a \rightarrow a')$ denotes the rate coefficient for collisions induced by heavy plasma ions with number density N_h . The radiative transition rate $A_r(a \rightarrow a')$ contributes only when the argument of the unit step function Θ is greater than zero. In the present investigation, the Bethe approximation,²¹ given by Eq. (21), has been employed to take into account all electron collisional processes which correspond to electric dipole transitions; and the radiative transition rates have also been included, even though their effect is negligible for these $\Delta n = 0$ transitions. The most important electron collisional processes correspond to dipole transitions involving a change in the orbital-angular-momentum quantum number of one of the outer electrons, and the relevant transition energies are large enough to justify our neglect of ion-induced collisions.

If we ignore self-absorption of the satellite radiation²⁵ by the plasma, the total rate of radiative emission per unit volume in the satellite transition $a \rightarrow f$ may be expressed in the form¹⁵

$$I(a \rightarrow f) = \sum_i \alpha_{DR}(i \epsilon_i \rightarrow a \rightarrow f) N(i) N_e + \sum_b C_r(b \rightarrow a \rightarrow f) N(b) N_e, \quad (23)$$

which represents an extension of Eq. (4) to take into account the transition rates given by Eq. (22). The generalized emission rate coefficient for dielectronic recombination radiation is obtained in the form

$$\alpha_{DR}(i \epsilon_i \rightarrow a \rightarrow f) = \sum_{a'} A_r(a \rightarrow f) Q^{-1}(a, a') C_{cap}(i \epsilon_i \rightarrow a'), \quad (24)$$

while for the radiation which is emitted following collisional excitation of an inner-shell electron, the analogous result is given by

$$C_r(b \rightarrow a \rightarrow f) = \sum_{a'} A_r(a \rightarrow f) Q^{-1}(a, a') C_e(b \rightarrow a'). \quad (25)$$

The nondiagonal elements of the transition rate matrix Q are defined by

$$Q(a, a') = -W(a' \rightarrow a), \quad a \neq a' \quad (26)$$

while the diagonal elements are given by

$$Q(a, a) = \sum_i A_a(a \rightarrow i \epsilon_i) + \sum_f A_r(a \rightarrow f) + \sum_f N_e C_e(a \rightarrow f) + \sum_{a' \neq a} W(a \rightarrow a'). \quad (27)$$

Radiative corrections can now be included by introducing into the above equations the effective autoionization and radiative decay rates defined in Sec. II.

B. Dielectronic satellite-line shapes

For the accurate theoretical prediction of the entire K -shell radiative emission spectrum, it is necessary to determine the spectral intensities for all dielectronic satellites which are associated with the resonance lines of the hydrogenlike and heliumlike ions. In addition, the analysis of the Stark-broadened²⁶ profiles for resolvable satellite lines may provide a spectroscopic determination of the densities in laser-compressed plasmas. For very dense plasmas and for blended fine-structure components, it may be necessary to employ an overlapping line-shape theory. We have investigated the entire K -shell satellite spectrum arising from the $n=2$ transitions in the isolated-line approximation. Our objective has been to systematically take into account all satellite lines arising from the radiative decay of the autoionizing states $2l'2l''$ and $1s 2l'2l''$, allowing for electron-impact broadening. A future extension of this investigation will be devoted to the inclusion of the quasistatic Stark broadening resulting from the ion-produced electric microfields.

In the isolated-line approximation,²⁷ the emission spectrum produced by the radiatively stabilizing transitions $a \rightarrow f$ can be represented in the form

$$\varepsilon(\omega) = \frac{\hbar\omega}{4\pi} \sum_a \sum_f N(a) A_r(a \rightarrow f) L(a \rightarrow f, \omega), \quad (28)$$

which gives the power radiated per unit volume and per unit solid angle and angular frequency intervals. In the absence of Doppler broadening, $L(a \rightarrow f, \omega)$ are the frequency-normalized Lorentzian line-shape functions, which are characterized by frequency-dependent linewidths $\Gamma_{af}(\omega)$ and shifts $\Delta_{af}(\omega)$. However, these frequency dependencies have been neglected in our calculations. We have evaluated the lowest-order nonvanishing contributions to the linewidths which arise from all permissible autoionization and spontaneous radiative emission processes as well as from both elastic and inelastic electron collisions. A self-consistent treatment has been accomplished by taking into account all of these atomic processes in the determination of the population densities $N(a)$ of the autoionizing levels.

The entire emission spectrum produced by the dielectronic satellite transitions in a plasma may be represented, according to Eq. (28), as a sum of convolution integrals involving the Lorentzian line-shape functions and the Doppler-broadening functions. In a future investigation, the Lorentzian line shapes will be evaluated as functions of a quasistatic ion-produced electric field and then convolved with a suitable electric microfield distribution function to provide the complete Stark-broadened profiles for the dielectronic satellite lines.

It is well known that autoionizing states are not true eigenstates of the unperturbed atomic Hamiltonian H_A . However, they may be treated as eigenstates of the projected Hamiltonian $(1-P)H_A(1-P)$, where P denotes the projection operator introduced by Feshbach.²⁸ The operator P projects a given atomic state onto the subspace of the open-channel electron-continuum states describing the nonresonant electron-ion collision process. The projected interaction $(1-P)H_A P$, which is responsible for autoioni-

zation, produces the asymmetric line shape first investigated by Fano.²⁹ It can be easily demonstrated that the asymmetric line-shape function reduces to a Lorentzian in the limit of large values of the Fano line-profile parameter Q_f . In the one-discrete-level two-continua model, the interference between the unperturbed autoionization and spontaneous radiative decay modes is important only for small values of Q_f . In the more complex cases of many autoionization or radiative decay modes,^{7,11} this interference effect can be significant even for large values of Q_f . Knowledge of the Q_f values for all radiatively stabilizing transitions is clearly required for the precise determination of the dielectronic satellite spectrum.

The evaluation of the satellite linewidth Γ_{af} to the lowest nonvanishing order in the various interactions leads to the result²⁷

$$\Gamma_{af} = \Gamma_{af}^{\text{AP}} + \Gamma_{af}^{\text{SR}} + \Gamma_{af}^{\text{IR}} + \Gamma_{af}^{\text{EC}}, \quad (29)$$

which is simply the sum of the partial linewidths arising from autoionization processes (AP), spontaneous and induced radiative (SR, IR) transitions, and electron collisions (EC). The partial linewidth due to autoionization is most generally given by

$$\Gamma_{af}^{\text{AP}} = \sum_i A_a(a \rightarrow i\epsilon_i) + \sum_j A_a(f \rightarrow j\epsilon_j), \quad (30)$$

which is the sum of the autoionization rates connecting the upper and lower levels a and f with the respective open electron-continuum channels, $i\epsilon_i$ and $j\epsilon_j$. For the radiatively stabilizing transitions considered in the present investigation, the lower levels f are not subject to autoionization. The partial linewidth due to spontaneous radiative transitions is given by

$$\Gamma_{af}^{\text{SR}} = \sum_{f'} A_r(a \rightarrow f') + \sum_{f'} A_r(f \rightarrow f'), \quad (31)$$

which is the sum of the spontaneous emission rates from the upper and lower levels comprising the satellite line $a \rightarrow f$. The partial linewidth Γ_{af}^{IR} can be expressed in terms of the transition rates for the induced radiative emission and absorption processes. The induced radiative processes have not been included in the present calculations. The inclusion of the electromagnetic interaction between the unperturbed autoionization and spontaneous radiative decay channels produces a small reduction¹² in the combined natural width $\Gamma_{af}^{\text{AP}} + \Gamma_{af}^{\text{SR}}$.

The evaluation of the lowest-order nonvanishing contributions to the partial linewidth describing binary electron-ion collisions leads to the result²⁷

$$\begin{aligned} \Gamma_{af}^{\text{EC}} = & \sum_{a'} N_e C_e(a \rightarrow a') + \sum_{f'} N_e C_e(f \rightarrow f') \\ & + \left\langle \int d\Omega N_e V_e |f_a(\Omega) - f_f(\Omega)|^2 \right\rangle_{\text{av}}, \end{aligned} \quad (32)$$

which is the sum of the inelastic transition rates $N_e C_e(a \rightarrow a')$ and $N_e C_e(f \rightarrow f')$ depleting the upper and lower levels and the average $\langle \cdot \rangle_{\text{av}}$, over the distribution of electron velocities V_e , of an integral involving the square of the difference between the elastic scattering amplitudes $f_a(\Omega)$ and $f_f(\Omega)$. It should be emphasized that this relationship has been derived within the framework of the im-

pact and binary-collision approximations,²⁶ in which the duration of an electron-ion collision is assumed to be short compared with the radiative lifetime and the radiating atomic system is assumed to interact only with a single perturbing electron during the collision process. The expression (32) for the collisional contribution to the satellite linewidth is clearly analogous to the formula for bound-bound radiative transitions which has been derived by Baranger.³⁰⁻³²

The systematic determination of the complete K -shell dielectronic satellite-line spectrum would appear to require the acquisition of an enormous amount of atomic energy-level and transition-probability data. Even for the simplest case of the $2l'2l'' \rightarrow 1s 2l$ satellite transitions in heliumlike ions, the number of $J_a \rightarrow J_f$ fine-structure components which are permissible according to the electric dipole selection rules is 22. It is particularly important to introduce simplifying approximations for the large number of electron collisional transition rates which are needed in the calculations. The collisional transitions between the closely spaced $n=2$ levels are expected to be the dominant inelastic scattering processes. The Bethe approximation given by Eq. (21) should provide an adequate representation for these electron-ion collision rates in the most important region of the scattering cross sections, which corresponds to incident electron energies that are several times the threshold values. The Bethe approximation obviously cannot be employed for collisional processes which do not correspond to electric dipole transitions. For collisional processes connecting autoionizing levels in heliumlike and lithiumlike ions, the dipole transition rates have been found^{15,24} to be at least 2 orders of magnitude larger than the nondipole transition rates in the important temperature region.

In order to obtain the total linewidth describing electron-impact broadening, it is necessary to evaluate the elastic scattering contribution. Griem³³ has estimated the elastic scattering term by extrapolating the electric dipole collisional excitation cross sections to zero values of the incident electron energy. It is apparent that this extrapolation procedure can provide an estimate for only the resonant elastic scattering process, which corresponds to autoionization following radiationless electron capture.³⁴ Both the ordinary nonresonant elastic collision contribution as well as the interference term in Eq. (32) are ignored in this extrapolation procedure. Nevertheless, we have tentatively adopted this method of estimating the elastic scattering contribution in our calculations. A more detailed evaluation will require a very great effort.

IV. DESCRIPTION AND RESULTS OF THE CALCULATIONS

Provided that self-absorption of the dielectronic satellite radiation²⁵ can be neglected, the entire satellite spectra produced by the $n=2$ transitions can be determined from the generalized emission rate coefficients for dielectronic recombination and inner-shell-electron collisional excitation together with the total linewidths resulting from all autoionization processes, spontaneous radiative transitions, and electron collisions. The total satellite-line in-

tensities, which are the result of both electron excitation mechanisms, have been evaluated by utilizing the population densities of the ground and singly excited bound states that have been determined by a detailed collisional radiative equilibrium model.²⁴

A. Unperturbed decay rates and electron collisional rate coefficients

The $n=2$ autoionizing levels together with electric dipole radiatively stabilizing transitions are schematically illustrated by the energy-level diagrams shown in Figs. 1 and 2 for the heliumlike and lithiumlike ions, respectively. The various fine-structure components of the satellite transitions in the heliumlike ion have been identified according to a numerical scheme, which differs from the abbreviated notation employed by Duston *et al.*²⁴ For the classification of the satellite lines in the lithiumlike ion, the widely used alphabetical designation first introduced by Gabriel¹³ has been adopted. Since relativistic corrections to the radiative- and radiationless-transition operators can be taken into account only when the atomic states are represented according to the total electronic angular momentum J , it is necessary to employ the J representation in order to investigate relativistic and radiative corrections to the spectral-line intensities.

In the absence of the final-state continuum-continuum

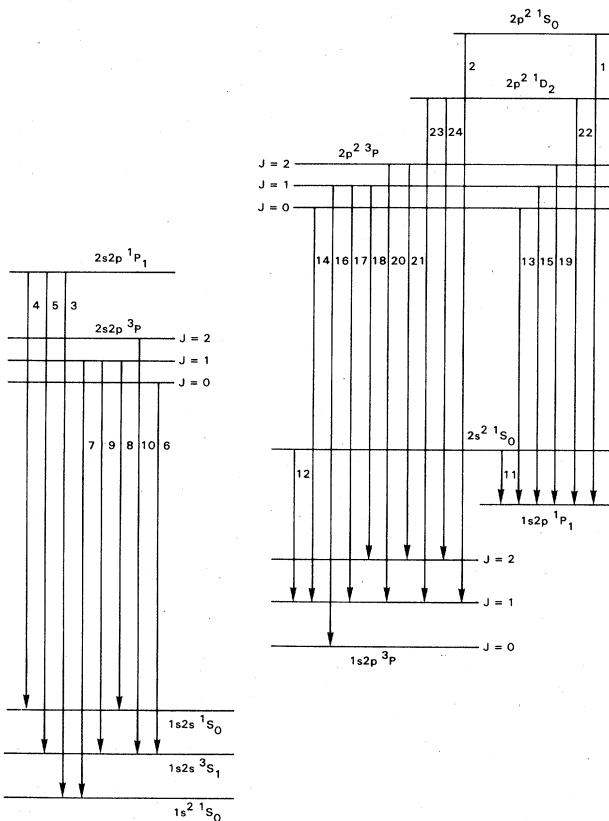


FIG. 1. $2l'2l''$ autoionizing levels of the heliumlike ion and the electric dipole radiative transitions which produce satellite lines in the vicinity of the $2p \rightarrow 1s$ resonance line from the hydrogenlike ion.

interaction, the autoionization and spontaneous radiative decay rates may be evaluated by means of the familiar expressions⁷

$$A_a(a \rightarrow i\varepsilon_i) = \frac{2\pi}{\hbar(2J_a+1)}$$

$$\times \sum_{k,l} |\langle \gamma_a J_a || V || \gamma_i J_i, K\varepsilon_i l; J_a \rangle|^2 \quad (33)$$

and

$$A_r(a \rightarrow f) = \frac{4e^2 \omega^3}{3\hbar C^3} \frac{|\langle \gamma_a J_a || D || \gamma_f J_f \rangle|^2}{2J_a+1}. \quad (34)$$

The continuum-continuum coupling parameters can be expressed in the form

$$\Psi = 1 + \frac{\alpha^2}{2\pi a_0^2} \sum_f \left(\frac{\hbar\omega}{E_H} \right)^2 \frac{2J_f+1}{2J_a+1} \sigma_p(f \rightarrow i\varepsilon_i; J_a), \quad (35)$$

where the partial photoionization cross sections are given by

$$\sigma_p(f \rightarrow i\varepsilon_i; J_a) = \frac{4\pi^2 \alpha \hbar \omega}{3(2J_f+1)}$$

$$\times \sum_{K,l} |\langle \gamma_i J_i, K\varepsilon_i l; J_a || D || \gamma_f J_f \rangle|^2. \quad (36)$$

In order to evaluate the radiative corrections for the most complex multichannel processes, it is necessary to determine the Fano line-profile parameter by using the general definition²⁰

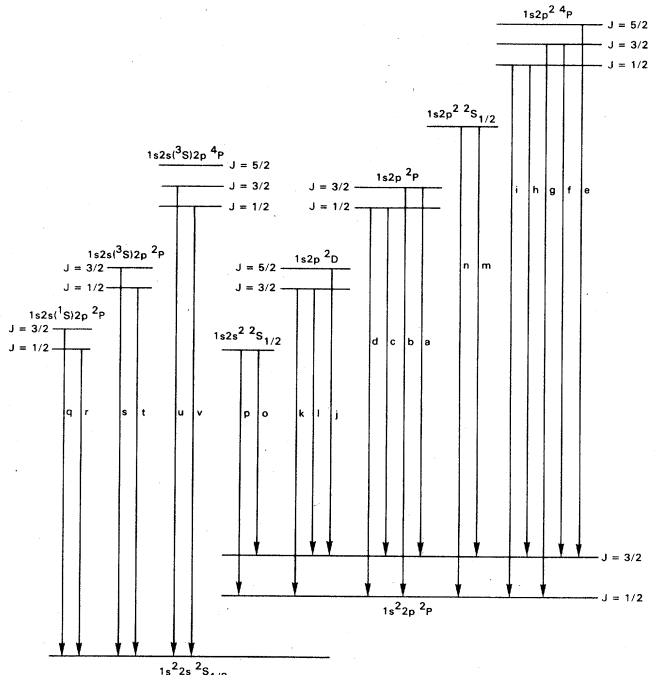


FIG. 2. $1s2l'2l''$ autoionizing levels of the lithiumlike ion and the electric dipole radiative transitions which produce satellite lines in the vicinity of the $1s2p 1P_1 \rightarrow 1s^2 1S_0$ resonance line from the heliumlike ion.

$$Q_f = \frac{(2J_a + 1) |\langle \gamma_a J_a || \mathbf{D} || \gamma_f J_f \rangle|}{\sum_{K,l} \langle \gamma_a J_a || V || \gamma_i J_i, K \epsilon_i l; J_a \rangle \langle \gamma_i J_i, K \epsilon_i l; J_a || \mathbf{D} || \gamma_f J_f \rangle}, \quad (37)$$

which involves the phases of the various interaction matrix elements.

The effective interaction V between electrons can be described, in the lowest nonvanishing order of quantum electrodynamical perturbation theory, by a second-order process which involves the virtual emission and absorption of a photon. If the radiation field is specified using the Lorentz gauge, the evaluation of the second-order S matrix yields the effective interaction operator in the Møller form³⁵

$$V = \sum_{i,j} (1 - \alpha_i \cdot \alpha_j) \frac{\exp(ikr_{ij})}{r_{ij}}, \quad (38)$$

which includes both the retarded Coulomb interaction and the relativistic current-current interaction. The Dirac matrices are denoted by α_i , and the wave number of the virtual photon is designated by k . If the radiation field is alternatively specified using the Coulomb gauge, the effective interaction operator V can be written as the sum of the electrostatic and generalized Breit operators.

The electric dipole moment operator \mathbf{D} describes the first-order process which results in the emission of a photon in the atomic transition $a \rightarrow f$. The first-order S matrix can be evaluated by well-known techniques³⁵ using the relativistic atom-field interaction

$$H_{AF} = -e \left[\frac{2\pi\hbar}{\omega_k} \right]^{1/2} \sum_j \alpha_j \cdot \hat{\epsilon}_{k\lambda}^* e^{-ik \cdot r_j}, \quad (39)$$

which includes both the retarded electromagnetic interaction and the relativistic current density. If the plane-wave radiation field is expanded in spherical waves, describing photon states of definite angular momentum and parity, and only the electric-dipole contribution is retained, the relativistic dipole operator which is obtained in the length gauge can be reduced, in the long-wavelength limit, to the familiar nonrelativistic length form.

The unperturbed autoionization and radiative decay rates employed in this investigation have been calculated using two different relativistic atomic structure codes. The majority of the autoionization and radiative decay rates and all of the photoionization cross sections were obtained by evaluating matrix elements of the nonrelativistic forms of the transition operators between multiconfiguration intermediate-coupling eigenstate expansions which were generated by the atomic structure code developed by Cowan.³⁶ The atomic wave functions provided by this atomic structure code are solutions of equations in the Hartree-Fock form, which incorporate some of the lowest-order relativistic corrections within the framework of a nonrelativistic procedure. For autoionization from the $2p^2 3P_1$ and $1s 2s 2p^4 P_{5/2}$ metastable states, which can only occur by means of the spin-spin interaction, it is necessary to evaluate a relativistic form of the radiationless transition operator using solutions of the Dirac-Hartree-Fock equations.³⁷ The fully relativistic Auger

code created by Chen³⁸ has been employed for this purpose.

The unperturbed autoionization and radiative decay rates, together with the photon wavelengths and the Fano line-profile parameters, are presented in Tables I and II for radiatively stabilizing transitions from the $2l'2l'$ and the $1s2l'2l''$ autoionizing states, respectively. There is no entry for the $1s 2s 2p^4 P_{5/2}$ metastable state, from which radiative decay can only occur by means of a very weak magnetic quadrupole transition. The Fano line-profile parameters for the quartet autoionizing states of the lithium-like ion are not presented; they are defined in terms of matrix elements for spin-forbidden photoelectric transitions, for which nonvanishing results cannot be obtained by using the approximation available for the electron-continuum wave functions. For most of the intense satellite lines, the relativistic corrections to the electric dipole radiative decay rates are found to be less than 5%. However, the relativistic corrections to the autoionization rates are found to be more significant, particularly when autoionization cannot occur by means of the instantaneous Coulomb interaction.

The electron collisional rate coefficients obtained using the Bethe approximation for dipole transitions between the $2l'2l''$ autoionizing states are presented in Table III, and the corresponding results for the $1s2l'2l''$ autoionizing states are tabulated in Table IV. The collisional rate coefficients for selected transitions are compared with the results obtained from more elaborate distorted-wave calculations²⁴ for heliumlike and lithiumlike ions in Figs. 3 and 4, respectively. The differences revealed by these comparisons are probably within the expected accuracy of both scattering approximations. The Bethe approximation has also been employed to evaluate the rates for collisional excitation of an inner-shell electron, and selected comparisons between the results obtained from the Bethe and distorted-wave calculations are illustrated for heliumlike and lithiumlike ions in Figs. 5 and 6, respectively. In this case the agreement between the results obtained by the two different methods is closer than anticipated; the Bethe approximation is questionable for transitions involving large energy differences, for which the threshold region of the cross sections provides the dominant contribution to the excitation rates in the most important temperature range. In order to obtain more accurate results for the electron collisional rates, it will probably be necessary to perform fully relativistic coupled-channel calculations, in which the collision channels corresponding to all $n=2$ bound excited and autoionizing states are included in the electron-continuum wave function expansions.

B. Effects of radiative corrections in low-density plasmas

The unperturbed autoionization and radiative decay rates together with the parameters Q_f and Ψ have been

TABLE I. Unperturbed decay rates and Q_f values for the satellite transitions $2l'2l'' \rightarrow 1s2l$ in heliumlike argon (Ar XVII). Numbers in parentheses are powers of ten.

Radiatively stabilizing transition $a \rightarrow f$	Abbreviated notation	Photon wavelength $\lambda(\text{\AA})$	Autoionization rate $A_a(a \rightarrow i\varepsilon_i)$ (sec $^{-1}$)	Radiative decay rate $A_r(a \rightarrow f)$ (sec $^{-1}$)	Fano line-profile parameter Q_f
$2s^2 1S_0 \rightarrow 1s2p^1P_1$	1	3.808	3.39(14)	2.23(13)	1.35(2)
$2s^2 1S_0 \rightarrow 1s2p^3P_1$	2	3.790	3.39(14)	2.44(12)	-3.91(2)
$2s2p^1P_1 \rightarrow 1s^2 1S_0$	3	1.928	1.90(14)	2.31(10)	-6.64(-1)
$2s2p^1P_1 \rightarrow 1s2s^1S_0$	4	3.753	1.90(14)	6.30(13)	-1.29(2)
$2s2p^1P_1 \rightarrow 1s2s^3S_1$	5	3.732	1.90(14)	3.28(11)	-5.49(2)
$2s2p^3P_0 \rightarrow 1s2s^3S_1$	6	3.765	1.98(13)	6.41(13)	4.04(2)
$2s2p^3P_1 \rightarrow 1s^2 1S_0$	7	1.936	1.78(13)	1.31(8)	-6.92(-1)
$2s2p^3P_1 \rightarrow 1s2s^1S_0$	8	3.785	1.78(13)	3.56(11)	-1.35(2)
$2s2p^3P_1 \rightarrow 1s2s^3S_1$	9	3.763	1.78(13)	6.26(13)	-4.33(2)
$2s2p^3P_2 \rightarrow 1s2s^3S_1$	10	3.760	1.45(13)	6.28(13)	-4.66(2)
$2p^2 1S_0 \rightarrow 1s2p^1P_1$	11	3.742	1.91(13)	1.06(14)	-1.22(3)
$2p^2 1S_0 \rightarrow 1s2p^3P_1$	12	3.724	1.91(13)	4.87(10)	2.29(2)
$2p^2 3P_0 \rightarrow 1s2p^1P_1$	13	3.784	1.14(12)	6.94(11)	4.09(2)
$2p^2 3P_0 \rightarrow 1s2p^3P_1$	14	3.766	1.14(12)	1.25(14)	4.80(4)
$2p^2 3P_1 \rightarrow 1s2p^1P_1$	15	3.782	7.71(10)	5.03(11)	-9.60(3)
$2p^2 3P_1 \rightarrow 1s2p^3P_0$	16	3.763	7.71(10)	4.17(13)	-1.71(4)
$2p^2 3P_1 \rightarrow 1s2p^3P_1$	17	3.764	7.71(10)	3.08(13)	9.01(3)
$2p^2 3P_1 \rightarrow 1s2p^3P_2$	18	3.768	7.71(10)	5.23(13)	-5.08(4)
$2p^2 3P_2 \rightarrow 1s2p^1P_1$	19	3.779	2.05(13)	3.88(12)	1.45(2)
$2p^2 3P_2 \rightarrow 1s2p^3P_1$	20	3.762	2.05(13)	3.26(13)	-2.96(3)
$2p^2 3P_2 \rightarrow 1s2p^3P_2$	21	3.765	2.05(13)	8.86(13)	4.35(4)
$2p^2 1D_2 \rightarrow 1s2p^1P_1$	22	3.769	3.27(14)	1.19(14)	1.99(2)
$2p^2 1D_2 \rightarrow 1s2p^3P_1$	23	3.752	3.27(14)	5.28(8)	-1.17(0)
$2p^2 1D_2 \rightarrow 1s2p^3P_2$	24	3.755	3.27(14)	5.28(12)	1.51(4)

TABLE II. Unperturbed decay rates and Q_f values for the satellite transitions $1s2l'2l'' \rightarrow 1s^2 2l$ in lithiumlike argon (Ar XVI). Numbers in parentheses are powers of ten.

Radiatively stabilizing transition $a \rightarrow f$	Abbreviated notation	Photon wavelength $\lambda(\text{\AA})$	Autoionizing rate $A_a(a \rightarrow i\varepsilon_i)$ (sec $^{-1}$)	Radiative decay rate $A_r(a \rightarrow f)$ (sec $^{-1}$)	Fano line-profile parameter Q_f
$1s2p^{22}P_{3/2} \rightarrow 1s^2 2p^2P_{3/2}$	<i>a</i>	3.985	1.01(13)	1.48(14)	3.27(3)
$1s2p^{22}P_{3/2} \rightarrow 1s^2 2p^2P_{1/2}$	<i>b</i>	3.981	1.01(13)	9.54(12)	-1.17(3)
$1s2p^{22}P_{1/2} \rightarrow 1s^2 2p^2P_{3/2}$	<i>c</i>	3.990	1.56(11)	4.60(13)	-1.12(4)
$1s2p^{22}P_{1/2} \rightarrow 1s^2 2p^2P_{1/2}$	<i>d</i>	3.986	1.56(11)	1.19(14)	2.54(4)
$1s2p^{24}P_{5/2} \rightarrow 1s^2 2p^2P_{3/2}$	<i>e</i>	4.011	1.60(12)	6.29(11)	
$1s2p^{24}P_{3/2} \rightarrow 1s^2 2p^2P_{3/2}$	<i>f</i>	4.013	5.23(10)	3.37(11)	
$1s2p^{24}P_{3/2} \rightarrow 1s^2 2p^2P_{1/2}$	<i>g</i>	4.009	5.23(10)	2.21(9)	
$1s2p^{24}P_{1/2} \rightarrow 1s^2 2p^2P_{3/2}$	<i>h</i>	4.015	4.70(7)	7.80(9)	
$1s2p^{24}P_{1/2} \rightarrow 1s^2 2p^2P_{1/2}$	<i>i</i>	4.010	4.70(7)	3.94(11)	
$1s2p^{22}D_{5/2} \rightarrow 1s^2 2p^2P_{3/2}$	<i>j</i>	3.992	1.25(14)	5.29(13)	2.26(2)
$1s2p^{22}D_{3/2} \rightarrow 1s^2 2p^2P_{1/2}$	<i>k</i>	3.989	1.16(14)	6.32(13)	8.91(2)
$1s2p^{22}D_{3/2} \rightarrow 1s^2 2p^2P_{3/2}$	<i>l</i>	3.993	1.16(14)	3.51(11)	-4.70(1)
$1s2p^{22}S_{1/2} \rightarrow 1s^2 2p^2P_{3/2}$	<i>m</i>	3.967	2.04(13)	4.45(13)	-9.54(2)
$1s2p^{22}S_{1/2} \rightarrow 1s^2 2p^2P_{1/2}$	<i>n</i>	3.963	2.04(13)	8.63(12)	-5.91(2)
$1s2s^{22}S_{1/2} \rightarrow 1s^2 2p^2P_{3/2}$	<i>o</i>	4.070	1.08(14)	3.13(12)	-1.12(2)
$1s2s^{22}S_{1/2} \rightarrow 1s^2 2p^2P_{1/2}$	<i>p</i>	4.066	1.08(14)	1.98(12)	-1.26(2)
$1s2s(^1S_0)2p^2P_{3/2} \rightarrow 1s^2 2s^2S_{1/2}$	<i>q</i>	3.981	2.40(12)	1.05(14)	-1.53(3)
$1s2s(^1S_0)2p^2P_{1/2} \rightarrow 1s^2 2s^2S_{1/2}$	<i>r</i>	3.984	1.28(13)	8.88(13)	6.36(1)
$1s2s(^3S_1)2p^2P_{3/2} \rightarrow 1s^2 2s^2S_{1/2}$	<i>s</i>	3.968	8.27(13)	6.29(12)	-6.09(2)
$1s2s(^3S_1)2p^2P_{1/2} \rightarrow 1s^2 2s^2S_{1/2}$	<i>t</i>	3.969	7.23(13)	2.30(13)	1.30(2)
$1s2s2p^4P_{3/2} \rightarrow 1s^2 2s^2S_{1/2}$	<i>u</i>	4.013	1.00(10)	4.71(11)	
$1s2s2p^4P_{1/2} \rightarrow 1s^2 2s^2P_{1/2}$	<i>v</i>	4.014	1.00(10)	1.63(11)	

TABLE III. Electron collisional rate coefficients for transitions between the autoionizing states $2l'2l''$ in heliumlike argon (Ar XVII), evaluated at $k_B T_e = 1.6$ keV in the Bethe approximation. Numbers in parentheses are powers of ten.

Transition $a \rightarrow a'$	Energy-level separation $\Delta E(a \rightarrow a')$ (Ry)	Excitation rate coefficient $C_e(a' \rightarrow a)$ ($\text{cm}^3 \text{ sec}^{-1}$)	Dexcitation rate coefficient $C_e(a \rightarrow a')$ ($\text{cm}^3 \text{ sec}^{-1}$)
$2s 2p^1 P_1 \rightarrow 2s 2^1 S_0$	2.35	8.97(-10)	3.05(-10)
$2s 2p^3 P_1 \rightarrow 2s 2^1 S_0$	3.22(-1)	1.39(-16)	4.66(-17)
$2p^2 1^1 S_0 \rightarrow 2s 2p^1 P_1$	1.90	6.80(-10)	2.07(-9)
$2p^2 3^1 P_0 \rightarrow 2s 2p^1 P_1$	8.13(-1)	9.99(-12)	3.02(-11)
$2p^2 3^1 P_1 \rightarrow 2s 2p^1 P_1$	6.90(-1)	1.30(-12)	1.31(-12)
$2p^2 3^1 P_2 \rightarrow 2s 2p^1 P_1$	5.16(-1)	6.81(-11)	4.10(-11)
$2p^2 1^1 D_2 \rightarrow 2s 2p^1 P_1$	1.21(-1)	1.88(-9)	1.13(-9)
$2p^2 3^1 P_1 \rightarrow 2s 2p^3 P_0$	1.43	8.03(-10)	2.71(-10)
$2p^2 1^1 S_0 \rightarrow 2s 2p^3 P_1$	3.93	1.22(-13)	3.79(-13)
$2p^2 3^1 P_0 \rightarrow 2s 2p^3 P_1$	1.21	2.81(-10)	8.51(-10)
$2p^2 3^1 P_1 \rightarrow 2s 2p^3 P_1$	1.33	2.02(-10)	2.04(-10)
$2p^2 3^1 P_2 \rightarrow 2s 2p^3 P_1$	1.51	3.34(-10)	2.02(-10)
$2p^2 1^1 D_2 \rightarrow 2s 2p^3 P_1$	2.14	2.85(-12)	1.74(-10)
$2p^2 3^1 P_1 \rightarrow 2s 2p^3 P_2$	1.11	2.10(-10)	3.54(-10)
$2p^2 3^1 P_2 \rightarrow 2s 2p^3 P_2$	1.28	5.79(-10)	5.85(-10)
$2p^2 1^1 D_2 \rightarrow 2s 2p^3 P_2$	1.92	3.36(-11)	3.42(-11)

employed to evaluate the effective decay rates, in the presence of the final-state continuum-continuum interaction, for the satellite transitions in Tables I and II, with the exception of the quartet autoionizing states of the lithium-

like ion. The perturbed autoionization rates are found to differ from their unperturbed values by less than 1%, but the radiatively stabilizing transition rates for certain satellite lines are significantly altered. The effects of the radiative corrections on the radiative transition rates and on the corresponding low-density dielectronic recombination rate coefficients are revealed by the comparisons presented in Tables V and VI, which list the unperturbed and modified values for the most strongly affected satellite transitions in heliumlike and lithiumlike argon, respectively. For this purpose we have evaluated the recombination rates at the representative temperature of $k_B T_e = 1.6$ keV, which is near the maximum emission temperature for the K-shell lines of argon in a corona equilibrium plasma. There is no appreciable temperature variation within a 0.5 keV range on either side of this maximum.

The perturbed and unperturbed values of the low-density dielectronic recombination rate coefficients for two strongly affected satellite transitions are compared as functions of temperature for heliumlike and lithiumlike argon in Figs. 7 and 8, respectively. Since these satellite transitions do not produce the most prominent spectral features in low-density plasmas, we are motivated to investigate the effects of radiative corrections in high-density plasmas, where the angular-momentum-changing collisions can dramatically enhance the intensities of radiative transitions from the metastable autoionizing levels. We conclude this subsection by presenting, in Figs. 9 and 10, the temperature variations of the intensities for the satellite lines in heliumlike and lithiumlike argon which are most prominent at low densities. The sum of the in-

TABLE IV. Electron collision rate coefficients for transitions between the autoionizing states $1s 2l'2l'$ in lithiumlike argon (Ar XVI), evaluated at $k_B T_e = 1.6$ keV in the Bethe approximation. Numbers in parentheses are powers of ten.

Transition $a \rightarrow a'$	Energy-level separation $\Delta E(a \rightarrow a')$ (Ry)	Excitation rate coefficient $C_e(a' \rightarrow a)$ ($\text{cm}^3 \text{ sec}^{-1}$)	Deexcitation rate coefficient $C_e(a \rightarrow a')$ ($\text{cm}^3 \text{ sec}^{-1}$)
$1s 2s(^1S_0)2p^2 P_{1/2} \rightarrow 1s 2s^2 2^1 S_{1/2}$	2.30	1.90(-12)	1.93(-12)
$1s 2s(^1S_0)2p^2 P_{3/2} \rightarrow 1s 2s^2 2^1 S_{1/2}$	2.43	7.25(-11)	3.70(-11)
$1s 2s(^3S_1)2p^2 P_{1/2} \rightarrow 1s 2s^2 2^1 S_{1/2}$	3.15	4.62(-10)	4.75(-10)
$1s 2s(^3S_1)2p^2 P_{3/2} \rightarrow 1s 2s^2 2^1 S_{1/2}$	3.21	8.54(-10)	4.39(-10)
$1s 2p^{2^2} S_{1/2} \rightarrow 1s 2s(^1S_0)2p^2 P_{1/2}$	3.52	1.36(-11)	1.40(-11)
$1s 2p^{2^2} S_{1/2} \rightarrow 1s 2s(^1S_0)2p^2 P_{3/2}$	3.39	2.67(-11)	5.49(-11)
$1s 2p^{2^2} S_{1/2} \rightarrow 1s 2s(^3S_1)2p^2 P_{1/2}$	2.68	5.32(-10)	5.44(-10)
$1s 2p^{2^2} S_{1/2} \rightarrow 1s 2s(^3S_1)2p^2 P_{3/2}$	2.61	5.17(-10)	1.06(-9)
$1s 2p^{2^2} P_{1/2} \rightarrow 1s 2s(^1S_0)2p^2 P_{1/2}$	2.23	5.24(-10)	5.33(-10)
$1s 2p^{2^2} P_{1/2} \rightarrow 1s 2s(^1S_0)2p^2 P_{3/2}$	2.09	1.44(-10)	2.92(-10)
$1s 2p^{2^2} P_{1/2} \rightarrow 1s 2s(^3S_1)2p^2 P_{1/2}$	1.38	1.80(-11)	1.82(-11)
$1s 2p^{2^2} P_{1/2} \rightarrow 1s 2s(^3S_1)2p^2 P_{3/2}$	1.31	2.76(-13)	5.58(-13)
$1s 2p^{2^2} P_{3/2} \rightarrow 1s 2s(^1S_0)2p^2 P_{1/2}$	2.47	2.59(-10)	1.32(-10)
$1s 2p^{2^2} P_{3/2} \rightarrow 1s 2s(^1S_0)2p^2 P_{3/2}$	2.34	5.19(-10)	5.30(-10)
$1s 2p^{2^2} P_{3/2} \rightarrow 1s 2s(^3S_1)2p^2 P_{1/2}$	1.62	1.05(-10)	5.33(-11)
$1s 2p^{2^2} P_{3/2} \rightarrow 1s 2s(^3S_1)2p^2 P_{3/2}$	1.56	1.11(-10)	1.13(-10)
$1s 2p^{2^2} D_{3/2} \rightarrow 1s 2s(^1S_0)2p^2 P_{1/2}$	2.02	8.76(-12)	4.46(-12)
$1s 2p^{2^2} D_{3/2} \rightarrow 1s 2s(^1S_0)2p^2 P_{3/2}$	1.89	1.12(-10)	1.13(-10)
$1s 2s^{2^2} D_{3/2} \rightarrow 1s 2s(^3S_1)2p^2 P_{1/2}$	1.17	1.42(-9)	7.18(-10)
$1s 2p^{2^2} D_{3/2} \rightarrow 1s 2s(^3S_1)2p^2 P_{3/2}$	1.11	8.34(-11)	8.42(-11)
$1s 2p^{2^2} D_{5/2} \rightarrow 1s 2s(^1S_0)2p^2 P_{3/2}$	1.94	9.80(-11)	6.64(-11)
$1s 2p^{2^2} D_{5/2} \rightarrow 1s 2s(^3S_1)2p^2 P_{3/2}$	1.17	1.26(-9)	8.49(-10)

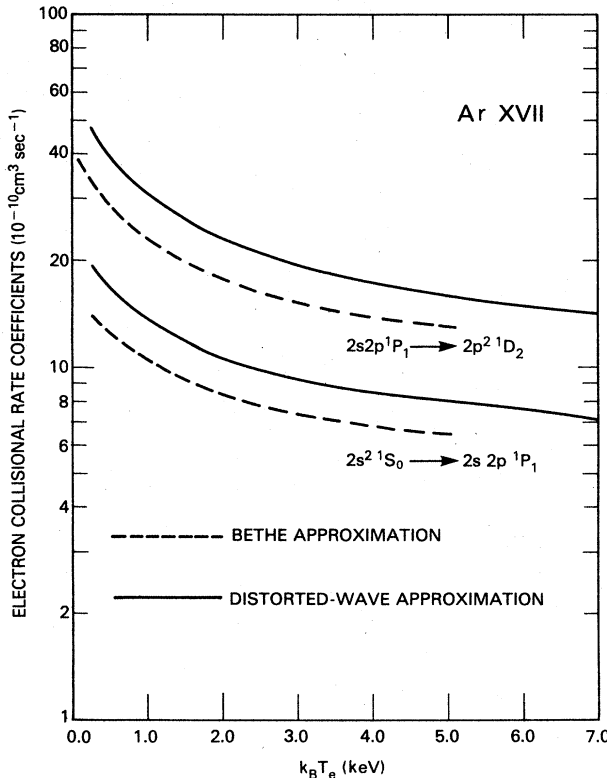


FIG. 3. Electron collisional rate coefficients for selected dipole transitions between the $2l'2l''$ autoionizing states in helium-like argon, evaluated in the Bethe approximation and compared with the results obtained from distorted-wave calculations (Ref. 24).

tensities has been plotted for satellite lines which are expected to overlap. Dielectronic recombination is the predominant production mechanism for the heliumlike satellite lines in low-density plasmas, but inner-shell-electron collisional excitation is important for the q , r , s , and t satellite lines in the lithiumlike ion.

TABLE V. Effects of the final-state interaction for selected dielectronic recombination satellite transitions in heliumlike argon (Ar XVII) at low electron densities. Numbers in parentheses are powers of ten.

Radiatively stable transition $a \rightarrow f$	Abbreviated notation	$A_r(a \rightarrow f)$	Radiative decay rates (sec^{-1}) $\bar{A}_r(a \rightarrow f)$	Dielectronic recombination radiation rate coefficients ($\text{cm}^3 \text{ sec}^{-1}$) for $k_B T_e = 1.6 \text{ keV}$ and $N_e = 10^{10} \text{ cm}^{-3}$ $\alpha_{DR}(i\epsilon_i \rightarrow a \rightarrow f)$	Dielectronic recombination radiation rate coefficients ($\text{cm}^3 \text{ sec}^{-1}$) for $k_B T_e = 1.6 \text{ keV}$ and $N_e = 10^{10} \text{ cm}^{-3}$ $\tilde{\alpha}_{DR}(i\epsilon_i \rightarrow a \rightarrow f)$
$2s2p^1P_1 \rightarrow 1s^2 1S_0$	3	2.31(10)	1.4(11)	1.59(-17)	7.17(-17)
$2s2p^3P_1 \rightarrow 1s^2 1S_0$	7	1.31(8)	5.16(9)	2.69(-20)	1.06(-18)
$2s2p^3P_1 \rightarrow 1s2s^1S_0$	8	3.56(11)	3.69(11)	7.33(-17)	7.59(-17)
$2p^2 1S_0 \rightarrow 1s2p^3P_1$	12	4.87(10)	4.59(10)	2.23(-18)	2.10(-18)
$2p^2 3P_0 \rightarrow 1s2p^1P_1$	13	6.94(11)	3.74(11)	1.93(-18)	1.05(-18)
$2p^2 3P_1 \rightarrow 1s2p^1P_1$	15	5.03(11)	6.87(11)	2.85(-19)	3.86(-19)
$2p^2 3P_1 \rightarrow 1s2p^3P_0$	16	4.17(13)	4.99(13)	2.37(-17)	2.80(-17)
$2p^2 3P_1 \rightarrow 1s2p^3P_1$	17	3.08(13)	2.06(13)	1.75(-17)	1.16(-17)
$2p^2 3P_1 \rightarrow 1s2p^3P_2$	18	5.23(13)	5.56(13)	2.97(-17)	3.12(-17)
$2p^2 3P_2 \rightarrow 1s2p^1P_1$	19	3.88(12)	3.57(12)	8.40(-16)	7.72(-16)
$2p^2 1D_2 \rightarrow 1s2p^3P_1$	23	5.28(8)	1.31(9)	5.85(-19)	1.46(-18)

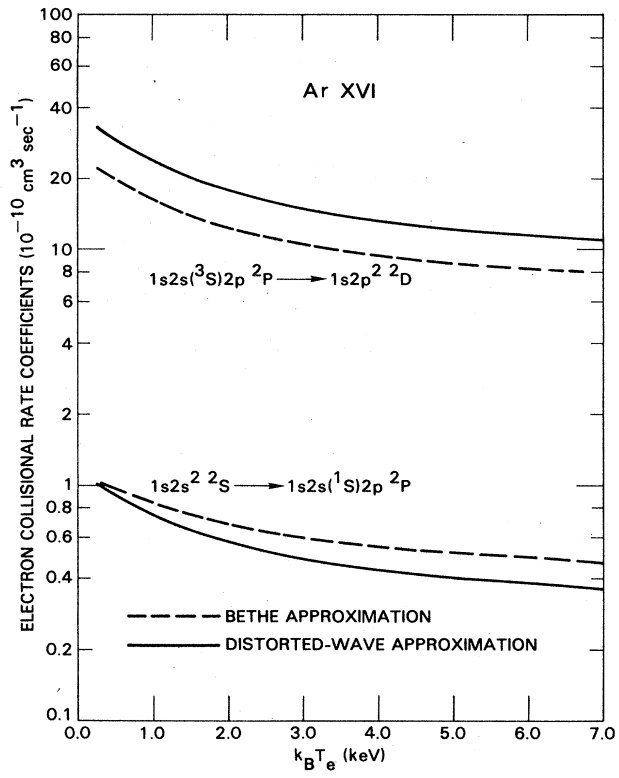


FIG. 4. Electron collisional rate coefficients for selected dipole transitions between the $1s2l'2l''$ autoionizing states in lithium-like argon, evaluated in the Bethe approximation and compared with the results obtained from distorted-wave calculations (Ref. 24).

C. Inclusion of collisional transitions between autoionizing levels

The generalized dielectronic recombination and inner-shell-electron collisional excitation rates for the most intense satellite lines are presented in Tables VII-X as

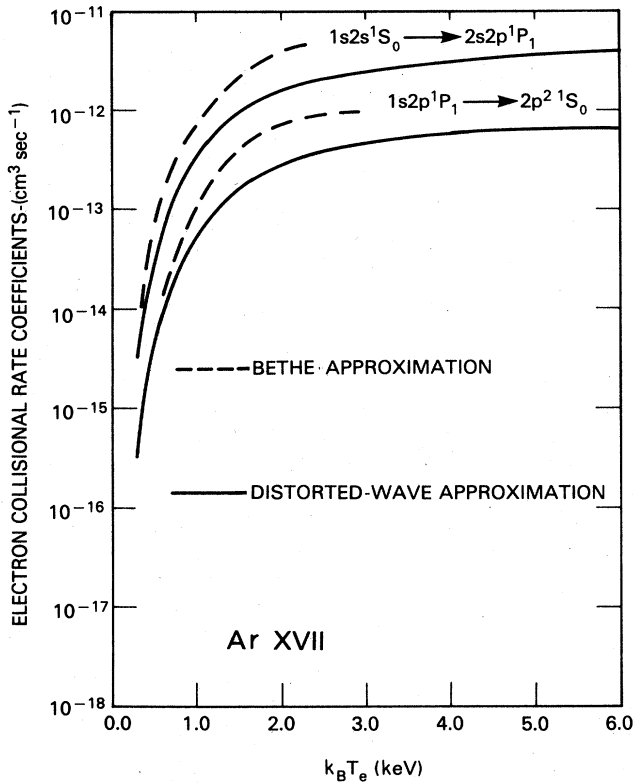


FIG. 5. Inner-shell-electron collisional excitation rate coefficients for selected dipole transitions to the $2l'2l''$ autoionizing states in heliumlike argon, evaluated in the Bethe approximation and compared with the results obtained from distorted-wave calculations (Ref. 24).

functions of density at the maximum K -shell emission temperature. The most spectacular effect of the angular-momentum-changing electron collisions is the sharp rise with increasing density in the intensities of radiative transitions from the $2p^23P_1$ and $1s2p^22P$ metastable autoionizing levels, which can not be significantly populated by the radiationless electron-capture process acting alone.

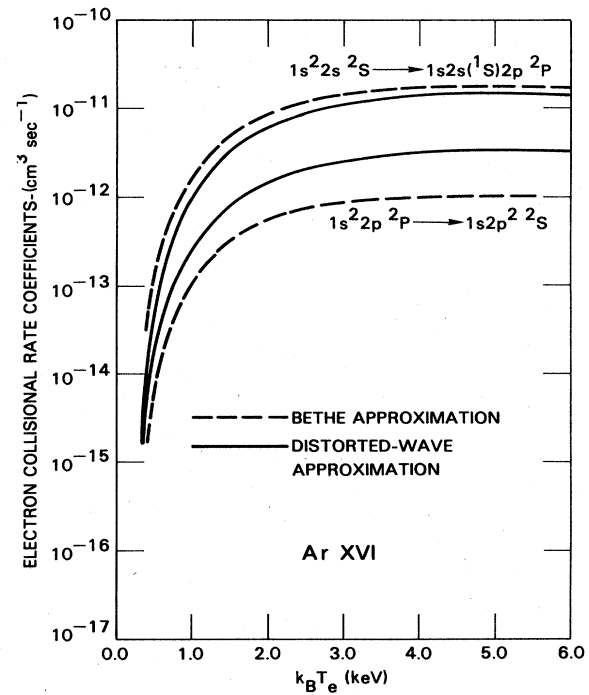


FIG. 6. Inner-shell-electron collisional excitation rate coefficients for selected dipole transitions to the $1s 2l'2l''$ autoionizing states in lithiumlike argon, evaluated in the Bethe approximation and compared with the results obtained from distorted-wave calculations (Ref. 24).

The intensities of these satellite transitions are predicted to be relatively weak at low densities, because the alternative inner-shell-electron excitation mechanism is efficient only when the excited bound states have appreciable population densities. In contrast, only a very weak density dependence is predicted for the intensities of radiative transitions from the strongly autoionizing $2p^21D_2$ and $1s2p^22D$ states, which give rise to prominent spectral features at all densities.

It may be possible to determine the density of a laser-compressed plasma from the satellite-intensity ratios

TABLE VI. Effects of the final-state interaction for selected dielectronic recombination satellite transitions in lithiumlike argon (Ar XVI) at low electron densities. Numbers in parentheses are powers of ten.

Radiatively stabilizing transition $a \rightarrow f$	Abbreviated notation	Radiative decay rates (sec ⁻¹)		Dielectronic recombination radiation rate coefficients (cm ³ sec ⁻¹) for $k_B T_e = 1.6$ keV and $N_e = 10^{10}$ cm ⁻³	
		$A_r(a \rightarrow f)$	$\tilde{A}_r(a \rightarrow f)$	$\alpha_{DR}(i\epsilon_i \rightarrow a \rightarrow f)$	$\tilde{\alpha}_{DR}(i\epsilon_i \rightarrow a \rightarrow f)$
$1s2p^{22}S_{1/2} \rightarrow 1s^22p^2P_{1/2}$	n	8.63(12)	8.65(12)	3.18(-15)	3.19(-15)
$1s2p^{22}P_{1/2} \rightarrow 1s^22p^2P_{1/2}$	d	1.19(14)	1.10(14)	1.49(-16)	1.38(-16)
$1s2p^{22}P_{3/2} \rightarrow 1s^22p^2P_{1/2}$	b	9.54(12)	9.86(12)	1.48(-15)	1.53(-15)
$1s2p^{22}P_{1/2} \rightarrow 1s^22p^2P_{3/2}$	c	4.60(13)	5.56(13)	5.76(-17)	6.93(-17)
$1s2p^{22}P_{3/2} \rightarrow 1s^22p^2P_{3/2}$	a	1.48(14)	1.47(14)	2.30(-14)	2.29(-14)
$1s2p^{22}D_{3/2} \rightarrow 1s^22p^2P_{3/2}$	l	3.51(11)	3.60(11)	5.88(-16)	6.03(-16)

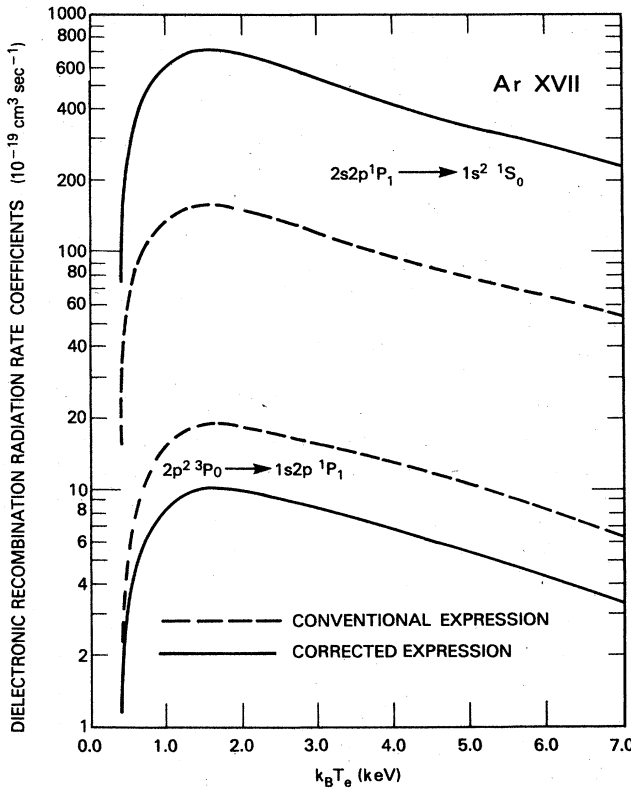


FIG. 7. Effects of radiative corrections on the low-density ($N_e = 10^{10} \text{ cm}^{-3}$) values of the dielectronic recombination radiation rate coefficients for selected satellite transitions in helium-like argon.

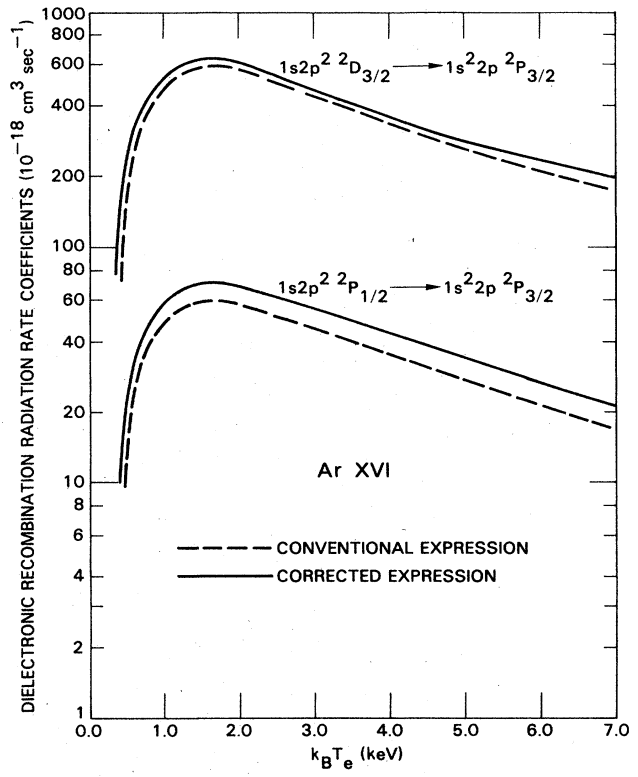


FIG. 8. Effects of radiative corrections on the low-density ($N_e = 10^{10} \text{ cm}^{-3}$) values of the dielectronic recombination radiation rate coefficients for selected satellite transitions in lithium-like argon.

TABLE VII. Dielectronic recombination radiation rate coefficients $\alpha_{DR}(i\varepsilon_i \rightarrow a \rightarrow f)$ ($\text{cm}^3 \text{ sec}^{-1}$) for the most intense $2l'2l'' \rightarrow 1s2l$ satellite transitions in heliumlike argon (Ar XVII), evaluated at $k_B T_e = 1.6 \text{ keV}$ and for representative electron densities N_e . Numbers in parentheses are powers of ten.

Radiatively stabilizing transition $a \rightarrow f$ (abbreviated notation)	$N_e = 10^{10} \text{ cm}^{-3}$	$N_e = 10^{20} \text{ cm}^{-3}$	$N_e = 10^{23} \text{ cm}^{-3}$	$N_e = 5.0 \times 10^{23} \text{ cm}^{-3}$	$N_e = 10^{24} \text{ cm}^{-3}$
1	6.48(-15)	6.48(-15)	6.16(-15)	5.49(-15)	5.06(-15)
4	4.33(-14)	4.33(-14)	4.06(-14)	3.91(-14)	3.74(-14)
6	4.71(-15)	4.70(-15)	3.02(-15)	2.95(-15)	3.47(-15)
9	1.28(-14)	1.28(-14)	9.60(-15)	9.95(-15)	1.13(-14)
10	1.83(-14)	1.82(-14)	1.67(-14)	1.87(-14)	2.11(-14)
11	4.87(-15)	4.90(-15)	1.58(-14)	1.97(-14)	1.97(-14)
14	3.47(-16)	3.53(-16)	3.07(-15)	5.60(-15)	7.01(-15)
16	2.79(-17)	3.43(-17)	2.98(-15)	6.02(-15)	7.78(-15)
17	1.15(-17)	1.42(-17)	1.23(-15)	1.49(-15)	3.22(-15)
18	3.12(-17)	3.83(-17)	3.33(-15)	6.72(-15)	8.68(-15)
19	7.72(-16)	7.72(-16)	8.75(-16)	1.04(-15)	1.18(-15)
20	7.10(-15)	7.10(-15)	8.05(-15)	9.56(-15)	1.08(-14)
21	1.92(-14)	1.92(-14)	2.18(-14)	2.58(-14)	2.93(-14)
22	1.31(-13)	1.30(-13)	1.30(-13)	1.24(-13)	1.18(-15)
24	5.86(-15)	5.86(-15)	5.79(-15)	5.54(-15)	5.29(-15)

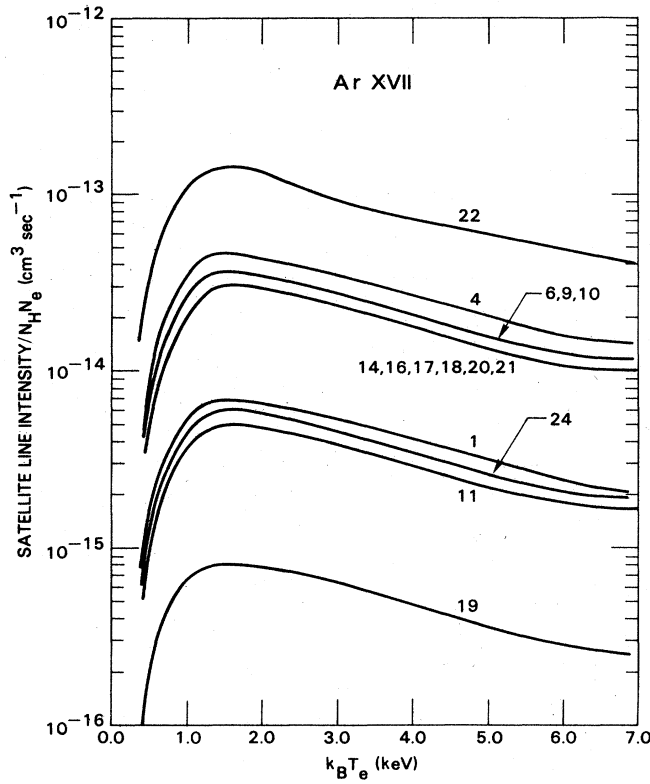


FIG. 9. Low-density ($N_e = 10^{10} \text{ cm}^{-3}$) values of the satellite-line intensities, per unit electron and hydrogenlike ion densities, evaluated for heliumlike argon taking into account both dielectronic recombination and inner-shell-electron collisional excitation. (The abbreviated notation is defined in Fig. 1.)

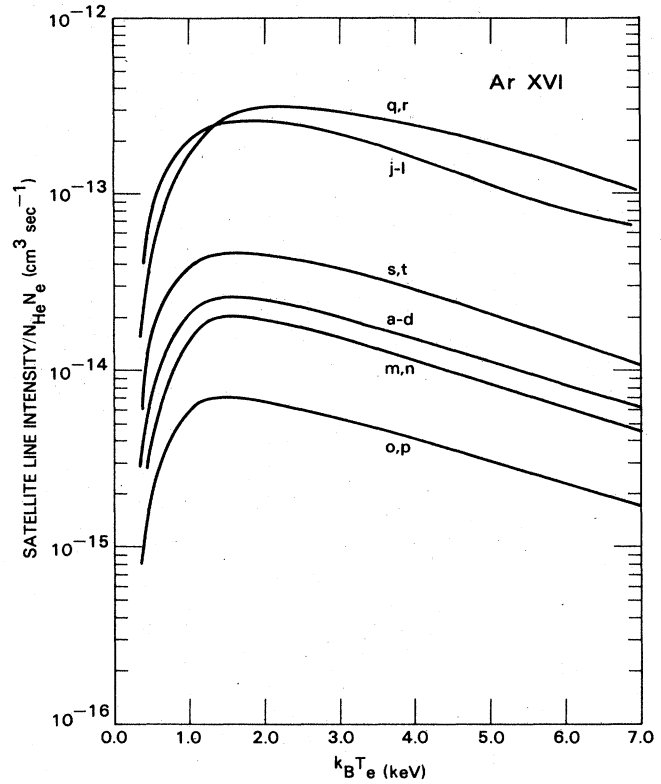


FIG. 10. Low-density ($N_e = 10^{10} \text{ cm}^{-3}$) values of the satellite-line intensities, per unit electron and heliumlike ion densities, evaluated for lithiumlike argon taking into account both dielectronic recombination and inner-shell-electron collisional excitation. (The abbreviated notation is defined in Fig. 2.)

TABLE VIII. Dielectronic recombination radiation rate coefficients $\alpha_{DR}(i\varepsilon_i \rightarrow a \rightarrow f)$ ($\text{cm}^3 \text{ sec}^{-1}$) for the most intense $1s2l'2l'' \rightarrow 1s^22l$ satellite transitions in lithiumlike argon (Ar XVI), evaluated at $k_B T_e = 1.6 \text{ keV}$ and for representative electron densities N_e . Numbers in parentheses are powers of ten.

Radiatively stabilizing transition $a \rightarrow f$ (abbreviated notation)	$N_e = 10^{10} \text{ cm}^{-3}$	$N_e = 10^{20} \text{ cm}^{-3}$	$N_e = 10^{23} \text{ cm}^{-3}$	$N_e = 5.0 \times 10^{23} \text{ cm}^{-3}$	$N_e = 10^{24} \text{ cm}^{-3}$
<i>a</i>	2.29(-14)	2.30(-14)	4.56(-14)	9.12(-14)	1.10(-13)
<i>b</i>	1.53(-15)	1.54(-15)	3.07(-15)	6.10(-15)	7.39(-15)
<i>c</i>	6.93(-17)	7.31(-17)	3.15(-15)	1.10(-14)	1.56(-14)
<i>d</i>	1.38(-16)	1.45(-16)	6.25(-15)	2.19(-14)	3.11(-14)
<i>j</i>	1.44(-13)	1.44(-13)	1.43(-13)	1.26(-13)	1.14(-13)
<i>k</i>	1.06(-13)	1.06(-13)	1.03(-13)	9.21(-14)	8.45(-14)
<i>l</i>	6.03(-16)	6.03(-16)	5.85(-16)	5.23(-16)	4.81(-16)
<i>m</i>	1.64(-14)	1.65(-14)	3.19(-14)	3.16(-14)	2.93(-14)
<i>n</i>	3.19(-15)	3.20(-15)	6.19(-15)	6.14(-15)	5.70(-15)
<i>o</i>	3.97(-15)	3.97(-15)	3.35(-15)	2.64(-15)	2.34(-15)
<i>p</i>	2.51(-15)	2.51(-15)	2.12(-15)	1.67(-15)	1.48(-15)
<i>q</i>	6.18(-15)	6.23(-15)	3.76(-14)	7.41(-14)	8.64(-14)
<i>r</i>	1.47(-14)	1.47(-14)	1.25(-14)	2.08(-14)	2.73(-14)
<i>s</i>	1.54(-14)	1.54(-14)	1.20(-14)	1.00(-14)	8.99(-15)
<i>t</i>	2.30(-14)	2.30(-14)	1.98(-14)	1.72(-14)	1.57(-14)

TABLE IX. Inner-shell-electron collisional excitation radiation rate coefficients $C_r(b \rightarrow a \rightarrow f)$ ($\text{cm}^3 \text{sec}^{-1}$) for the most intense $2l'2l'' \rightarrow 1s2l$ satellite transitions in heliumlike argon (Ar XVII), evaluated at $k_B T_e = 1.6 \text{ keV}$ and for representative electron densities N_e . Numbers in parentheses are powers of ten.

Radiatively stabilizing transition $a \rightarrow f$ (abbreviated notation)	$N_e = 10^{10} \text{ cm}^{-3}$	$N_e = 10^{20} \text{ cm}^{-3}$	$N_e = 10^{23} \text{ cm}^{-3}$	$N_e = 5.0 \times 10^{23} \text{ cm}^{-3}$	$N_e = 10^{24} \text{ cm}^{-3}$
$b = 1s 2s \ ^1S_0$					
1	5.80(-19)	2.20(-17)	9.40(-15)	1.46(-14)	1.51(-14)
4	7.22(-13)	7.21(-13)	3.94(-13)	2.20(-13)	1.77(-13)
6	5.45(-34)	9.76(-22)	3.89(-16)	3.38(-15)	6.41(-15)
9	1.38(-14)	1.37(-14)	1.08(-14)	1.74(-14)	2.50(-14)
10	3.03(-32)	4.28(-20)	8.95(-15)	3.17(-14)	4.67(-14)
11	6.61(-26)	6.59(-16)	1.35(-13)	1.08(-13)	9.20(-14)
14	1.74(-27)	1.74(-17)	6.44(-15)	1.23(-14)	1.71(-14)
16	2.34(-28)	2.33(-18)	1.84(-15)	9.51(-15)	1.64(-14)
17	9.69(-29)	9.67(-19)	7.62(-16)	3.93(-15)	6.81(-15)
18	2.61(-28)	2.60(-18)	2.05(-15)	1.06(-14)	1.83(-14)
19	2.09(-28)	2.09(-18)	8.80(-16)	1.96(-15)	2.72(-15)
20	1.92(-27)	1.92(-19)	8.09(-15)	1.80(-14)	2.50(-14)
21	5.21(-27)	5.20(-17)	2.19(-14)	4.87(-14)	6.77(-14)
22	5.71(-26)	5.70(-16)	2.47(-13)	3.77(-13)	3.88(-13)
24	2.54(-27)	2.54(-17)	1.10(-14)	1.68(-14)	1.73(-14)
$b = 1s 2s \ ^3S_1$					
1	9.74(-22)	3.69(-20)	1.09(-16)	1.06(-15)	2.12(-15)
4	1.21(-15)	1.21(-15)	4.60(-15)	1.60(-14)	2.48(-14)
6	2.55(-13)	2.55(-13)	1.60(-13)	1.08(-13)	8.99(-14)
9	7.57(-13)	7.56(-13)	4.60(-13)	3.05(-13)	2.53(-13)
10	1.32(-12)	1.32(-12)	7.71(-13)	4.93(-13)	4.06(-13)
11	1.23(-28)	1.23(-18)	1.61(-15)	7.91(-15)	1.29(-14)
14	3.36(-26)	3.35(-16)	1.19(-13)	1.49(-13)	1.39(-13)
16	3.96(-26)	3.95(-16)	1.43(-13)	1.81(-13)	1.69(-13)
17	1.64(-26)	1.63(-16)	5.93(-13)	7.49(-14)	7.00(-14)
18	4.42(-26)	4.41(-16)	1.60(-13)	2.02(-13)	1.88(-13)
19	3.97(-27)	3.96(-17)	1.48(-14)	1.94(-14)	1.84(-14)
20	3.65(-26)	3.64(-16)	1.36(-13)	1.78(-13)	1.69(-13)
21	9.88(-26)	9.87(-16)	3.69(-13)	4.83(-13)	4.59(-13)
22	2.05(-27)	2.05(-17)	1.19(-14)	4.33(-14)	7.08(-14)
24	9.14(-29)	9.54(-19)	5.32(-16)	1.92(-15)	3.15(-15)
$b = 1s 2p \ ^1P_1$					
1	7.56(-15)	7.56(-15)	9.24(-15)	1.47(-14)	1.66(-14)
4	3.04(-18)	4.26(-16)	1.33(-13)	1.70(-13)	1.69(-13)
6	1.00(-20)	1.80(-18)	1.13(-15)	5.25(-15)	9.17(-15)
9	1.14(-19)	1.38(-17)	6.91(-15)	2.10(-14)	3.24(-14)
10	4.01(-19)	5.30(-17)	2.31(-14)	4.95(-14)	6.72(-14)
11	4.55(-13)	4.54(-13)	2.16(-13)	1.32(-13)	1.13(-13)
14	1.98(-15)	1.98(-15)	4.17(-15)	1.36(-14)	2.13(-14)
16	4.32(-15)	4.32(-15)	5.35(-15)	1.47(-14)	2.35(-14)
17	1.78(-15)	1.78(-15)	2.21(-15)	6.10(-15)	9.74(-15)
18	4.82(-15)	4.82(-15)	5.96(-15)	1.64(-14)	2.62(-14)
19	2.32(-15)	2.32(-15)	2.08(-15)	2.96(-15)	3.85(-15)
20	2.13(-14)	2.13(-14)	1.91(-14)	2.72(-14)	3.54(-14)
21	5.78(-14)	5.77(-14)	5.18(-14)	7.37(-14)	9.60(-14)
22	8.23(-13)	8.23(-13)	7.35(-13)	6.49(-13)	5.99(-13)
24	3.66(-14)	3.66(-14)	3.27(-14)	2.89(-14)	2.66(-14)

TABLE IX. (Continued).

Radiatively stabilizing transition $a \rightarrow f$ (abbreviated notation)		$N_e = 10^{10} \text{ cm}^{-3}$ $N_e = 10^{20} \text{ cm}^{-3}$ $N_e = 10^{23} \text{ cm}^{-3}$ $N_e = 5.0 \times 10^{23} \text{ cm}^{-3}$ $N_e = 10^{24} \text{ cm}^{-3}$			
		$b = 1s\ 2p\ ^3P_0$			
1	2.66(-28)	1.82(-23)	2.83(-17)	5.75(-16)	1.34(-15)
4	3.31(-22)	5.99(-19)	1.19(-15)	8.66(-15)	1.57(-14)
6	2.13(-18)	3.83(-16)	1.29(-13)	1.22(-13)	9.85(-14)
9	1.31(-18)	2.93(-16)	1.11(-13)	1.61(-13)	1.58(-13)
10	1.30(-18)	5.31(-16)	1.94(-13)	2.65(-13)	2.57(-13)
11	5.21(-35)	5.96(-22)	4.16(-16)	4.27(-15)	8.18(-15)
14	5.81(-32)	1.29(-19)	2.90(-14)	7.88(-14)	8.70(-14)
16	9.17(-13)	9.17(-13)	6.12(-13)	3.45(-13)	2.53(-13)
17	3.79(-13)	3.79(-13)	2.53(-13)	1.42(-13)	1.04(-13)
18	1.02(-12)	1.02(-12)	6.82(-13)	3.84(-13)	2.82(-13)
19	4.68(-33)	1.58(-20)	3.70(-15)	1.04(-14)	1.16(-14)
20	4.31(-33)	1.45(-19)	3.40(-14)	9.58(-14)	1.07(-13)
21	1.16(-31)	3.93(-19)	9.22(-14)	2.59(-13)	2.90(-13)
22	2.04(-33)	8.32(-21)	3.02(-15)	2.33(-14)	4.48(-14)
24	9.10(-35)	3.70(-22)	1.34(-16)	1.04(-15)	1.99(-15)
		$b = 1s\ 2p\ ^3P_1$			
1	8.08(-16)	8.08(-16)	7.57(-16)	1.10(-15)	1.62(-15)
4	6.23(-21)	1.08(-17)	4.58(-15)	1.11(-14)	1.62(-14)
6	2.94(-19)	5.29(-17)	2.23(-14)	3.77(-14)	3.88(-14)
9	1.91(-18)	4.74(-16)	1.62(-13)	1.76(-13)	1.54(-13)
10	1.28(-18)	3.52(-16)	1.35(-13)	1.94(-13)	1.91(-13)
11	1.91(-16)	1.91(-16)	1.65(-15)	5.49(-15)	8.46(-15)
14	6.45(-13)	6.45(-13)	4.19(-13)	2.28(-13)	1.64(-13)
16	1.26(-13)	1.26(-13)	1.05(-13)	1.06(-13)	9.98(-14)
17	5.24(-14)	5.23(-14)	4.36(-14)	4.38(-14)	4.13(-14)
18	1.41(-13)	1.41(-13)	1.17(-13)	1.18(-13)	1.11(-13)
19	2.08(-14)	2.08(-14)	1.64(-14)	1.39(-14)	1.24(-14)
20	1.91(-13)	1.91(-13)	1.51(-13)	1.28(-13)	1.14(-13)
21	5.18(-13)	5.18(-13)	4.09(-13)	3.47(-13)	3.09(-13)
22	8.87(-18)	8.88(-18)	4.54(-15)	2.54(-14)	4.33(-14)
24	3.95(-19)	3.95(-19)	2.02(-16)	1.13(-15)	1.93(-15)
		$b = 1s\ 2p\ ^3P_2$			
1	1.79(-27)	4.56(-22)	1.56(-16)	9.77(-16)	1.73(-15)
4	2.22(-21)	1.49(-17)	6.58(-15)	1.47(-14)	2.02(-14)
6	4.79(-19)	8.59(-17)	3.29(-14)	4.62(-14)	4.49(-14)
9	1.29(-18)	2.16(-16)	8.51(-14)	1.25(-13)	1.23(-13)
10	2.09(-18)	5.74(-16)	2.05(-13)	2.48(-13)	2.28(-13)
11	2.25(-34)	1.37(-20)	2.26(-15)	7.24(-15)	1.05(-14)
14	5.72(-32)	9.62(-20)	2.21(-14)	6.13(-14)	6.82(-14)
16	2.06(-13)	2.05(-13)	1.55(-13)	1.29(-13)	1.15(-13)
17	8.52(-14)	8.51(-14)	6.45(-14)	5.36(-14)	4.77(-14)
18	2.29(-13)	2.29(-13)	1.73(-13)	1.44(-13)	1.28(-13)
19	3.40(-14)	3.39(-14)	2.51(-14)	1.80(-14)	1.50(-14)
20	3.12(-13)	3.12(-13)	2.31(-13)	1.66(-13)	1.38(-13)
21	8.46(-13)	8.45(-13)	6.26(-13)	4.49(-13)	3.74(-13)
22	2.15(-14)	2.15(-14)	2.35(-14)	4.20(-14)	5.94(-14)
24	9.60(-16)	9.60(-16)	1.05(-15)	1.88(-15)	2.64(-15)

TABLE X. Inner-shell-electron collisional excitation radiation rate coefficients $C_r(b \rightarrow a \rightarrow f)$ ($\text{cm}^3 \text{sec}^{-1}$) for the most intense $1s2l'2l'' \rightarrow 1s^22l$ satellite transitions in lithiumlike argon (Ar XVI) evaluated at $k_B T_e = 1.6 \text{ keV}$ and for representative electron densities N_e . Numbers in parentheses are powers of ten.

Radiatively stabilizing transition $a \rightarrow f$ (abbreviated notation)	$N_e = 10^{10} \text{ cm}^{-3}$	$N_e = 10^{20} \text{ cm}^{-3}$	$N_e = 10^{23} \text{ cm}^{-3}$	$N_e = 5.0 \times 10^{23} \text{ cm}^{-3}$	$N_e = 10^{24} \text{ cm}^{-3}$
$b = 1s^22s \ ^2S_{1/2}$					
<i>a</i>	2.36(-25)	2.36(-15)	9.38(-13)	1.16(-12)	1.07(-12)
<i>b</i>	1.58(-16)	1.58(-16)	6.28(-14)	7.74(-14)	7.14(-14)
<i>c</i>	5.20(-26)	1.19(-16)	2.12(-13)	2.63(-13)	2.37(-13)
<i>d</i>	1.03(-15)	1.03(-15)	4.21(-13)	5.21(-13)	4.70(-13)
<i>j</i>	2.28(-26)	2.28(-16)	1.03(-13)	2.40(-13)	3.00(-13)
<i>k</i>	4.22(-26)	4.21(-16)	1.45(-13)	2.47(-13)	2.79(-13)
<i>l</i>	2.40(-28)	2.40(-18)	8.25(-16)	1.40(-15)	1.59(-15)
<i>m</i>	3.31(-26)	3.30(-16)	5.91(-14)	8.51(-14)	9.55(-14)
<i>n</i>	6.44(-27)	6.41(-17)	1.15(-14)	1.66(-14)	1.86(-14)
<i>o</i>	8.32(-19)	1.51(-17)	3.73(-15)	6.07(-15)	6.95(-15)
<i>p</i>	5.26(-19)	9.52(-18)	2.36(-15)	3.84(-15)	4.40(-15)
<i>q</i>	4.29(-12)	4.29(-12)	2.54(-12)	1.38(-12)	1.06(-12)
<i>r</i>	1.63(-12)	1.62(-12)	1.04(-12)	6.36(-13)	4.95(-13)
<i>s</i>	1.82(-14)	1.82(-14)	1.44(-14)	2.25(-14)	2.62(-14)
<i>t</i>	1.14(-13)	1.14(-13)	5.28(-14)	5.19(-14)	5.47(-14)
$b = 1s^22p \ ^2P_{1/2}$					
<i>a</i>	3.63(-13)	3.63(-13)	4.02(-13)	5.88(-13)	6.25(-13)
<i>b</i>	2.43(-14)	2.43(-14)	2.69(-14)	3.94(-14)	4.18(-14)
<i>c</i>	7.75(-13)	7.74(-13)	5.55(-13)	3.37(-13)	2.56(-13)
<i>d</i>	1.54(-12)	1.54(-12)	1.10(-12)	6.69(-13)	5.09(-13)
<i>j</i>	4.60(-13)	2.07(-19)	3.95(-14)	1.65(-13)	2.26(-13)
<i>k</i>	9.37(-13)	9.37(-13)	7.22(-13)	4.98(-13)	4.13(-13)
<i>l</i>	5.33(-15)	5.33(-15)	4.11(-15)	2.84(-15)	2.35(-15)
<i>m</i>	1.05(-13)	1.04(-13)	7.49(-14)	8.51(-14)	8.86(-14)
<i>n</i>	2.04(-14)	2.03(-14)	1.46(-14)	1.65(-14)	1.72(-14)
<i>o</i>	1.27(-15)	1.27(-15)	3.12(-15)	5.52(-14)	6.15(-15)
<i>p</i>	8.04(-16)	8.03(-16)	1.97(-15)	3.49(-15)	3.89(-15)
<i>q</i>	1.41(-17)	7.19(-16)	3.05(-13)	4.71(-13)	4.84(-13)
<i>r</i>	1.61(-17)	7.03(-16)	2.79(-13)	3.32(-13)	2.97(-13)
<i>s</i>	7.04(-19)	3.14(-17)	8.64(-15)	1.77(-14)	2.12(-14)
<i>t</i>	2.03(-18)	3.03(-16)	6.49(-14)	6.57(-14)	6.06(-14)
$b = 1s^22p \ ^2P_{3/2}$					
<i>a</i>	2.72(-12)	2.72(-12)	2.00(-12)	1.30(-12)	1.06(-12)
<i>b</i>	1.82(-13)	1.82(-13)	1.34(-13)	8.72(-14)	7.06(-14)
<i>c</i>	1.96(-13)	1.96(-13)	1.65(-13)	1.58(-13)	1.49(-13)
<i>d</i>	3.89(-13)	3.89(-13)	3.27(-13)	3.14(-13)	2.96(-13)
<i>j</i>	5.01(-13)	5.00(-13)	4.32(-13)	3.99(-13)	3.85(-13)
<i>k</i>	2.68(-15)	2.68(-15)	5.38(-14)	1.68(-13)	2.13(-13)
<i>l</i>	1.52(-17)	1.53(-17)	3.06(-16)	9.58(-16)	1.21(-15)
<i>m</i>	2.76(-13)	2.75(-13)	1.33(-13)	1.06(-13)	1.02(-13)
<i>n</i>	5.36(-14)	5.35(-14)	2.58(-14)	2.06(-14)	2.00(-14)
<i>o</i>	1.01(-15)	1.01(-15)	3.32(-15)	5.95(-15)	6.60(-15)
<i>p</i>	6.38(-16)	6.38(-16)	2.10(-15)	3.77(-15)	4.17(-15)
<i>q</i>	3.11(-17)	1.19(-15)	4.63(-13)	5.94(-13)	5.68(-13)
<i>r</i>	1.13(-17)	3.97(-16)	1.66(-13)	2.38(-13)	2.34(-13)
<i>s</i>	2.03(-18)	1.21(-16)	2.40(-14)	2.86(-14)	2.89(-14)
<i>t</i>	3.54(-18)	1.14(-16)	2.30(-14)	3.86(-14)	4.41(-14)

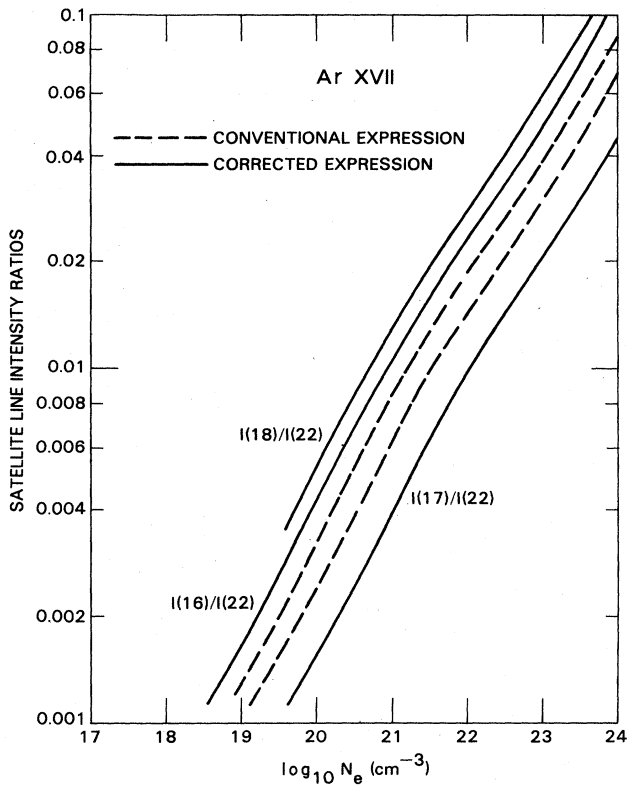


FIG. 11. Effects of angular-momentum-changing electron collisions and radiative corrections on selected satellite-line intensity ratios in heliumlike argon, evaluated at $k_B T_e = 1.6$ keV taking into account both dielectronic recombination and inner-shell-electron collisional excitation. (The abbreviated notation is defined in Fig. 1.)

$I(16)/I(22)$, $I(17)/I(22)$, $I(18)/I(22)$ and $I(a)/I(j)$, $I(b)/I(j)$, $I(c)/I(j)$, $I(d)/I(j)$, which are shown as functions of density at the maximum K-shell emission temperature in Figs. 11 and 12, respectively. We emphasize that these satellite-line intensity ratios are considerably easier to analyze than the widely used ratio of the satellite-line intensity relative to the resonance-line intensity, which may have a substantial contribution from unresolvable dielectronic recombination satellites. The importance of angular-momentum-changing electron collisions and radiative corrections is illustrated by the striking differences between the unperturbed and modified values which are predicted for several of these intensity ratios.

Angular-momentum-changing electron collisions are also predicted to significantly alter the satellite-line shapes in high-density plasmas. The total linewidth Γ_{af} resulting from all autoionization, radiative decay, and electron collision processes may be conveniently specified in terms of the Voigt line-profile parameter defined by³⁹

$$A(a \rightarrow f) = \frac{\Gamma_{af}}{4\pi \Delta\nu_D} , \quad (40)$$

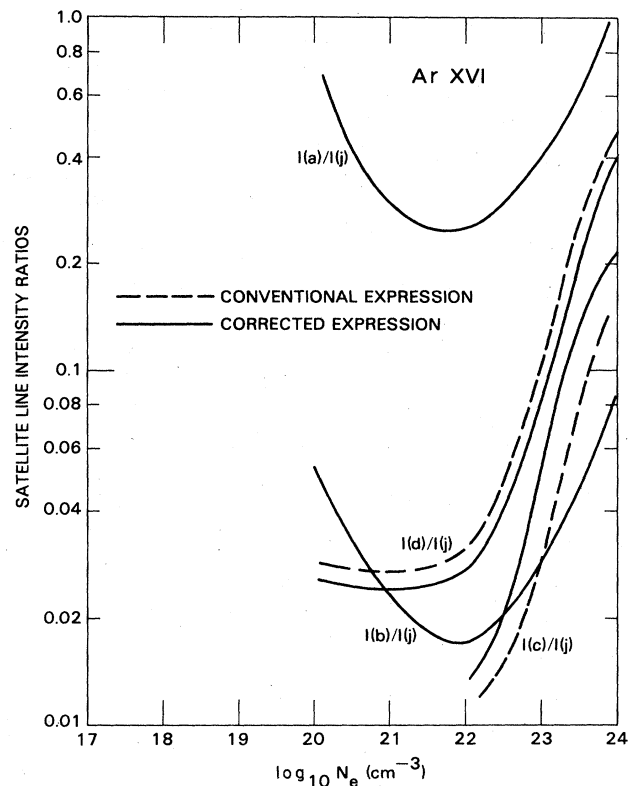


FIG. 12. Effects of angular-momentum-changing electron collisions and radiative corrections on selected satellite-line intensity ratios in lithiumlike argon, evaluated at $k_B T_e = 1.6$ keV taking into account both dielectronic recombination and inner-shell-electron collisional excitation. (The abbreviated notation is defined in Fig. 2.)

where $\Delta\nu_D$ denotes the thermal Doppler width. The Voigt line-profile parameters for the satellite transitions in the heliumlike and lithiumlike ions of argon are presented as functions of density in Tables XI and XII, respectively. The density behavior of this parameter for some of the most intense satellite lines is illustrated in Figs. 13 and 14. Doppler broadening is clearly seen to be the dominant mechanism determining the line shapes below $N_e = 10^{22} \text{ cm}^{-3}$, while the electron-impact broadening resulting from angular-momentum-changing transitions is predicted to prevail for densities beyond $N_e = 10^{24} \text{ cm}^{-3}$. The dramatic change in the satellite-emission spectra, which is predicted to occur in the density range $10^{22} \leq N_e \leq 10^{24} \text{ cm}^{-3}$, may provide a spectroscopic indication of plasma compression in laser-fusion experiments.

V. CONCLUSIONS

We have investigated the combined effects of radiative corrections and angular-momentum-changing electron collisions on the dielectronic satellite spectra arising from the entire array of radiatively stabilizing electric dipole transitions from the $n=2$ autoionizing states in the heliumlike and lithiumlike ions of argon. These effects are

TABLE XI. Voigt line-profile parameters for the satellite transitions $2l'2l'' \rightarrow 1s 2l$ in heliumlike argon (Ar XVII), evaluated at $k_B T_e = 1.6$ keV and for representative electron densities N_e . Numbers in parentheses are in powers of ten.

Radiatively stabilizing transition $a \rightarrow f$ (abbreviated notation)	$N_e = 10^{20} \text{ cm}^{-3}$	$N_e = 10^{22} \text{ cm}^{-3}$	$N_e = 10^{23} \text{ cm}^{-3}$	$N_e = 5.0 \times 10^{23} \text{ cm}^{-3}$	$N_e = 10^{24} \text{ cm}^{-3}$
1	1.65(-1)	1.70(-1)	2.13(-1)	4.04(-1)	6.42(-1)
2	1.26(-1)	1.30(-1)	1.72(-1)	3.59(-1)	5.91(-1)
3	4.45(-2)	4.96(-2)	9.67(-2)	3.06(-1)	5.67(-1)
4	8.66(-2)	1.01(-1)	2.33(-1)	8.21(-1)	1.55(0)
5	8.61(-2)	9.82(-2)	2.08(-1)	7.00(-1)	1.31(0)
6	2.88(-2)	3.37(-2)	7.88(-2)	2.79(-1)	5.29(-1)
7	1.43(-2)	1.57(-2)	2.91(-2)	8.86(-2)	1.63(-1)
8	2.79(-2)	3.52(-2)	1.03(-1)	4.01(-1)	7.74(-1)
9	2.77(-2)	3.27(-2)	7.83(-2)	2.81(-1)	5.34(-1)
10	2.65(-2)	3.15(-2)	7.71(-2)	2.80(-1)	5.33(-1)
11	8.19(-2)	9.05(-2)	1.68(-1)	5.15(-1)	9.48(-1)
12	4.31(-2)	5.16(-2)	1.28(-1)	4.70(-1)	8.97(-1)
13	8.32(-2)	8.78(-2)	1.30(-1)	3.16(-1)	5.49(-1)
14	4.40(-2)	4.85(-2)	8.95(-2)	2.72(-1)	4.99(-1)
15	8.32(-2)	8.77(-2)	1.28(-1)	3.07(-1)	5.32(-1)
16	4.34(-2)	4.78(-2)	8.72(-2)	2.62(-1)	4.81(-1)
17	4.40(-2)	4.84(-2)	8.78(-2)	2.63(-1)	4.82(-1)
18	4.35(-2)	4.65(-2)	7.40(-1)	1.96(-1)	3.48(-1)
19	8.96(-2)	9.41(-2)	1.34(-1)	3.13(-1)	5.37(-1)
20	5.04(-2)	5.48(-2)	9.41(-2)	2.69(-1)	4.87(-1)
21	4.99(-2)	5.29(-2)	8.03(-1)	2.02(-1)	3.54(-1)
22	1.94(-1)	2.00(-1)	2.50(-1)	4.76(-1)	7.58(-1)
23	1.54(-1)	1.60(-1)	2.09(-1)	4.31(-1)	7.07(-1)
24	1.54(-1)	1.58(-1)	1.96(-1)	3.64(-1)	5.74(-1)

TABLE XII. Voigt line-profile parameters for the satellite transitions $1s 2l'2l'' \rightarrow 1s^2 2l$ in lithiumlike argon (Ar XVI), evaluated at $k_B T_e = 1.6$ keV and for representative electron densities N_e . Numbers in parentheses are powers of ten.

Radiatively stabilizing transition $a \rightarrow f$ (abbreviated notation)	$N_e = 10^{20} \text{ cm}^{-3}$	$N_e = 10^{22} \text{ cm}^{-3}$	$N_e = 10^{23} \text{ cm}^{-3}$	$N_e = 5.0 \times 10^{23} \text{ cm}^{-3}$	$N_e = 10^{24} \text{ cm}^{-3}$
<i>a</i>	6.07(-2)	6.65(-2)	1.19(-1)	3.54(-1)	6.48(-1)
<i>b</i>	6.06(-2)	6.77(-2)	1.32(-1)	4.17(-1)	7.73(-1)
<i>c</i>	6.03(-2)	6.62(-2)	1.20(-1)	3.58(-1)	6.55(-1)
<i>d</i>	6.03(-2)	6.74(-2)	1.32(-1)	4.20(-1)	7.80(-1)
<i>j</i>	6.46(-2)	7.07(-2)	1.26(-1)	3.72(-1)	6.80(-1)
<i>k</i>	6.54(-2)	7.28(-2)	1.40(-1)	4.36(-1)	8.08(-1)
<i>l</i>	6.55(-2)	7.16(-2)	1.27(-1)	3.74(-1)	6.82(-1)
<i>m</i>	2.66(-2)	3.54(-2)	1.15(-1)	4.68(-1)	9.09(-1)
<i>n</i>	2.65(-2)	3.64(-2)	1.27(-1)	5.28(-1)	1.03(0)
<i>o</i>	4.21(-2)	5.02(-2)	1.23(-1)	4.49(-1)	8.56(-1)
<i>p</i>	4.21(-2)	5.14(-2)	1.36(-1)	5.13(-1)	9.83(-1)
<i>q</i>	3.90(-2)	4.71(-2)	1.20(-1)	4.43(-1)	8.47(-1)
<i>r</i>	3.69(-2)	4.44(-2)	1.13(-1)	4.17(-1)	7.97(-1)
<i>s</i>	3.21(-2)	4.55(-2)	1.66(-1)	7.00(-1)	1.37(-0)
<i>t</i>	3.46(-2)	4.83(-2)	1.73(-1)	7.29(-1)	1.42(0)

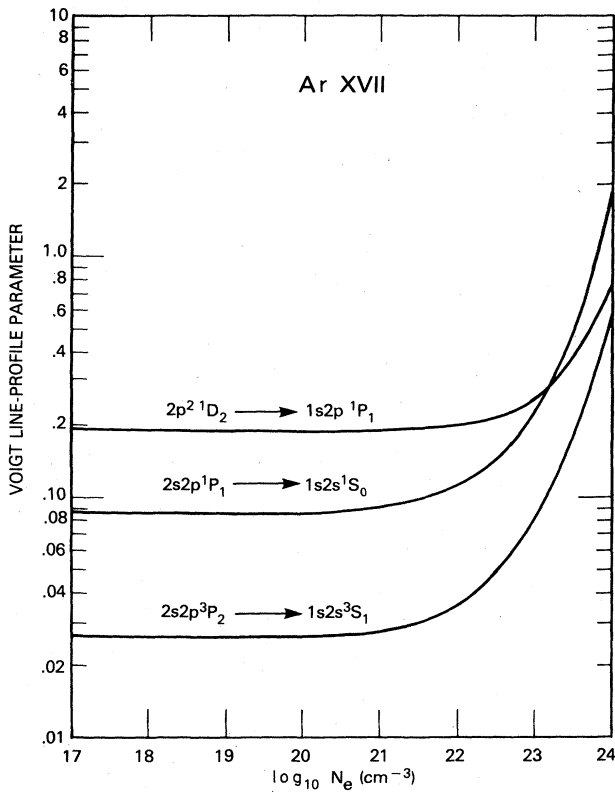


FIG. 13. Voigt line-profile parameters for selected satellite transitions $2l'2l'' \rightarrow 1s 2l$ in heliumlike argon, evaluated for $k_B T_e = 1.6$ keV.

predicted to be most significant for the satellite lines emitted from the $2p^2 3P_1$ and $1s 2p^2 2P$ metastable autoionizing states, which produce prominent spectral features in high-density plasmas. Provided that self-absorption of the satellite radiation can be neglected, it may be possible to utilize intensity ratios involving these satellite lines for the spectroscopic determination of compression in laser-produced plasmas.

In addition to the limitations imposed by the use of the isolated-resonance approximation and the neglect of the Stark broadening which results from the ion-produced electric microfield fluctuations, the fundamental theory of the satellite-line spectra may need further extension to remove the artificial distinction between the nonresonant radiative recombination and dielectronic recombination processes. Alber, Cooper, and Rau⁴⁰ have recently presented a unified treatment of radiative and dielectronic recombination which is based on the evaluation of the S matrix describing the entire collision process involving photon emission following electron capture, as first discussed by Davies and Seaton.⁸ This approach leads to the prediction of additional contributions to the satellite intensities which cannot be simply represented by Feynman-type diagrams involving intermediate autoionizing resonances. Apparently this unified treatment involves the abandonment of the Breit-Wigner resonance approximation.

The theory of dielectronic satellite spectra can also be

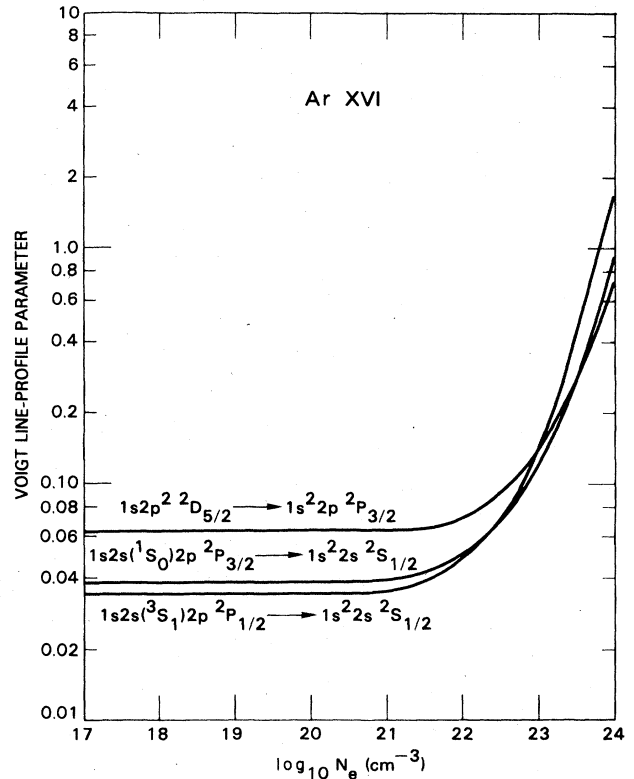


FIG. 14. Voigt line-profile parameters for selected satellite transitions $1s 2l'2l'' \rightarrow 1s^2 2l$ in lithiumlike argon, evaluated for $k_B T_e = 1.6$ keV.

further extended to allow for the effects of correlations (i.e., overlap in time) between the electron collision and spontaneous decay processes. The effects of correlations between collision and radiation processes have been treated within the framework of the density-matrix description by Ballagh and Cooper,⁴¹ who demonstrated that under suitable conditions the coherence terms can be neglected and the total transition rates can be expressed as sums of the rates that each individual mechanism would produce when acting alone. At very high densities for which many collisions can occur within the characteristic time for autoionization and radiative decay, the quantum-mechanical phases of the autoionizing states should become sufficiently randomized to justify the neglect of correlations between the collisional excitation and spontaneous decay processes.

ACKNOWLEDGMENTS

The authors are greatly indebted to Professor J. Cooper and Professor B. Crasemann for numerous stimulating discussions and continuous encouragement. Valuable discussions with Professor H. R. Griem, Dr. A. Hauer, Dr. M. Blaha, and Dr. D. Duston are gratefully acknowledged. This work has been supported by the U.S. Office of Naval Research and by the U.S. Department of Energy through the University of Rochester Laboratory for Laser Energetics.

- ¹A. Burgess, *Astrophys. J.* **139**, 776 (1964).
²A. B. Walker and H. R. Rugge, *Astrophys. J.* **164**, 181 (1971).
³G. A. Doschek, *Space Sci. Rev.* **13**, 765 (1972).
⁴N. J. Peacock, M. G. Hobby, and M. Galanti, *J. Phys. B* **6**, L298 (1973).
⁵U. Feldman, G. A. Doschek, D. N. Nagel, R. D. Cowan, and R. R. Whitlock, *Astrophys. J.* **192**, 213 (1974).
⁶V. L. Jacobs, *Astrophys. J.* **296**, 121 (1985).
⁷V. L. Jacobs, *Phys. Rev. A* **31**, 383 (1985).
⁸P. C. W. Davies and M. J. Seaton, *J. Phys. B* **2**, 757 (1969).
⁹R. H. Bell and M. J. Seaton, *J. Phys. B* **18**, 1589 (1985).
¹⁰B. W. Shore, *Rev. Mod. Phys.* **39**, 439 (1967).
¹¹L. Armstrong, Jr., C. E. Theodosiou, and M. J. Wall, *Phys. Rev. A* **18**, 2538 (1978).
¹²S. L. Haan and J. Cooper, *Phys. Rev. A* **28**, 3349 (1983).
¹³A. H. Gabriel, *Mon. Not. R. Astron. Soc.* **160**, 99 (1972).
¹⁴C. P. Bhalla, A. H. Gabriel, and L. P. Presnyakov, *Mon. Not. R. Astron. Soc.* **172**, 359 (1975).
¹⁵V. L. Jacobs and M. Blaha, *Phys. Rev. A* **21**, 525 (1980).
¹⁶A. Burgess and H. P. Summers, *Astrophys. J.* **157**, 1007 (1969).
¹⁷V. L. Jacobs and J. Davis, *Phys. Rev. A* **18**, 697 (1978).
¹⁸M. J. Seaton and P. J. Storey, in *Atomic Processes and Applications*, edited by P. G. Burke and B. L. Moiseiewitsch (North-Holland, Amsterdam, 1976), Chap. 6.
¹⁹V. L. Jacobs, J. Davis, and P. C. Kepple, *Phys. Rev. Lett.* **37**, 1390 (1976).
²⁰U. Fano and J. W. Cooper, *Phys. Rev.* **137**, A1364 (1965).
²¹H. A. Bethe, *Ann. Phys. (Leipzig)* **5**, 325 (1930).
²²A. V. Vinogradov, I. Yu Skobelev, and E. A. Yukov, *Zh. Eksp. Teor. Fiz.* **72**, 1762 (1977) [Sov. Phys.—JETP **45**, 925 (1977)].
²³J. F. Seely, *Phys. Rev. Lett.* **42**, 1606 (1979).
²⁴D. Duston, J. E. Rogerson, J. Davis, and M. Blaha, *Phys. Rev. A* **28**, 2968 (1983).
²⁵D. Duston and J. Davis, *Phys. Rev. A* **21**, 932 (1980).
²⁶H. R. Griem, *Spectral Line Broadening by Plasmas* (Academic, New York, 1974).
²⁷V. L. Jacobs and J. Davis, Naval Research Laboratory Memorandum Report No. 4365, 1980 (unpublished).
²⁸H. Feshbach, *Ann. Phys. (N.Y.)* **5**, 357 (1958).
²⁹U. Fano, *Phys. Rev.* **124**, 1866 (1961).
³⁰M. Baranger, *Phys. Rev.* **111**, 481 (1958).
³¹M. Baranger, *Phys. Rev.* **111**, 494 (1958).
³²M. Baranger, *Phys. Rev.* **111**, 855 (1958).
³³H. R. Griem, *Phys. Rev.* **165**, 258 (1968).
³⁴M. Blaha (private communication).
³⁵A. I. Akhiezer and V. B. Berestetskii, *Quantum Electrodynamics* (Interscience, New York, 1965).
³⁶R. D. Cowan and D. C. Griffin, *J. Opt. Soc. Am.* **66**, 1010 (1976).
³⁷I. P. Grant, B. J. McKenzie, P. H. Norrington, D. F. Mayers, and N. C. Pyper, *Comput. Phys. Commun.* **21**, 207 (1980).
³⁸M. H. Chen, *Phys. Rev. A* **31**, 1449 (1985).
³⁹D. Mihalas, *Stellar Atmospheres* (Freeman, San Francisco, 1970).
⁴⁰G. Alber, J. Cooper, and A. R. P. Rau, *Phys. Rev. A* **30**, 2845 (1984).
⁴¹R. J. Ballagh and J. Cooper, *J. Phys. B* **17**, 4411 (1984).